





RESEARCH ARTICLE | MAY 30 2023

## Experimental examination of the phase transition of water on silica at 298 K

Special Collection: [Chemical Physics of Controlled Wettability and Super Surfaces](#)

Sepehr Saber ; Nagarajan Narayanaswamy ; C. A. Ward; Janet A. W. Elliott  

 Check for updates

*J. Chem. Phys.* 158, 204712 (2023)

<https://doi.org/10.1063/5.0145932>



View  
Online

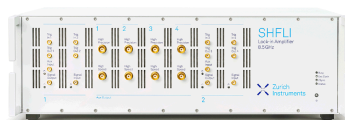


Export  
Citation

CrossMark

500 kHz or 8.5 GHz?  
And all the ranges in between.

Lock-in Amplifiers for your periodic signal measurements



Find out more

 Zurich  
Instruments

# Experimental examination of the phase transition of water on silica at 298 K

Cite as: J. Chem. Phys. 158, 204712 (2023); doi: 10.1063/5.0145932

Submitted: 8 February 2023 • Accepted: 30 April 2023 •

Published Online: 30 May 2023



View Online



Export Citation



CrossMark

Sepehr Saber,<sup>1</sup>  Nagarajan Narayanaswamy,<sup>1,a)</sup>  C. A. Ward,<sup>1</sup> and Janet A. W. Elliott<sup>2,b)</sup> 

## AFFILIATIONS

<sup>1</sup> Department of Mechanical Engineering, University of Toronto, Toronto, Ontario M5S 3G8, Canada

<sup>2</sup> Department of Chemical and Materials Engineering, University of Alberta, Edmonton, Alberta T6G 1H9, Canada

**Note:** This paper is part of the JCP Special Topic on Chemical Physics of Controlled Wettability and Super Surfaces.

<sup>a)</sup> Electronic mail: [nnagaraj@mie.utoronto.ca](mailto:nnagaraj@mie.utoronto.ca)

<sup>b)</sup> Author to whom correspondence should be addressed: [janet.elliott@ualberta.ca](mailto:janet.elliott@ualberta.ca)

## ABSTRACT

The objective of this study was to investigate the prediction of the wetting characteristics obtained from the equilibrium adsorption analysis using the Zeta adsorption isotherm approach with an experimental study. Water vapor's adsorption and wetting characteristics on a hydroxylated and nano-polished silica substrate were studied in near-equilibrium conditions at temperatures near 298 K. Using a UV-visible interferometer, water vapor adsorbate film thicknesses were measured and converted into amount adsorbed per unit area. The current results show that the wetting transition occurred at an average subcooling value of 0.39 K, less than the predicted value of 0.49 K. All the different experimental observations showed growth of film thickness as a function of subcooling value with a maximum film thickness of 12.6 nm. The analysis of the results further showed that the maximum stable film was in a metastable state that then condensed in a dropwise manner, if perturbed by increasing the subcooling. The study further revealed that the adsorbate is unstable after transitioning. The solid surface energy calculated by including the near-equilibrium observations was comparable and close to that of the equilibrium studies, thus supporting solid surface energy as a material property.

Published under an exclusive license by AIP Publishing. <https://doi.org/10.1063/5.0145932>

## I. INTRODUCTION

The phase transition of water is a natural phenomenon that impacts many aspects of our daily lives, from nature to industry. The transition of adsorbed water vapor into a condensed liquid phase is critical for fields such as material science, biology, industry, and climatology to name a few.<sup>1–5</sup> A deeper understanding of the condensation of water on silica is essential for the study of ice formation in clouds, drug delivery applications using mesoporous silica, formation of Pickering emulsions, and other industrial applications.<sup>6–11</sup> Studying the water–silica system is also important for understanding the toxicological potential of silica nanoparticles and aging of oxide surfaces.<sup>1,4,12–18</sup>

Although the vapor-to-liquid phase transition has been heavily studied in the past, the crucial role of adsorption and the precursor to phase transition has not always been given adequate

attention.<sup>19</sup> Recently, a new adsorption isotherm was developed using statistical thermodynamics, called the Zeta adsorption isotherm (ZAI),<sup>20</sup> and it has been shown to successfully describe the adsorption of vapor and gases on different substrate systems.<sup>20–31</sup> The central assumption of the ZAI approach is that the adsorbed molecules are organized into various types of clusters, which are modeled as quantum mechanical harmonic oscillators in a canonical ensemble.<sup>20</sup> Using this assumption, the ZAI approach was used to determine the thermodynamic isotherm of water vapor adsorption on a fully hydroxylated silica nanopowder<sup>31</sup> at 298 K. The wetting transition of the adsorbed vapor to liquid phase was predicted by extending the obtained thermodynamic isotherm<sup>31</sup> to near-equilibrium conditions and then determining the solid surface energy of silica,  $\gamma^{s0}$ , at 298 K. In this article, we want to examine whether the surface characterization of silica in the equilibrium range can be extended to the near-equilibrium

region using experimental techniques and examine whether the experimental results support the earlier prediction of wetting transition and  $\gamma^{S0}$ .

## II. ZETA ADSORPTION ISOTHERM

The applicability of equilibrium analysis of water adsorption on silica nanopowder using the ZAI has been demonstrated<sup>31</sup> based on the assumption that the adsorption takes place on a heterogeneity-free solid surface and that the adsorbate satisfies thermodynamic phase stability criteria.<sup>32</sup> The vapor adsorbate is modeled as consisting of molecular clusters<sup>20,30,32</sup> with each molecular cluster assumed to reside on one of the  $M$  adsorption sites per unit area of the adsorbent. The number of molecules a cluster can contain,  $\zeta$ , can be any positive integer value from zero to a maximum cluster size of  $\zeta_{th}$ . Furthermore, each cluster is approximated as a three-dimensional, quantum mechanical, harmonic oscillator with  $\omega^{(\zeta)}$  as the fundamental frequency, which depends on the number of molecules in the cluster.<sup>20</sup>

If system isothermal temperature is  $T^V$ , then the vapor-phase pressure ratio  $x^V$  is defined as

$$x^V = \frac{P^V}{P_{sat}(T^V)}, \quad (1)$$

where  $P^V$  is vapor-phase partial pressure and  $P_{sat}$  is the saturation pressure at  $T^V$ . If  $a_\zeta$  is the number of adsorbed clusters with  $\zeta$  molecules and when the adsorbate is in equilibrium with the vapor at a pressure ratio of  $x^V$  and at  $T^V$ , then the adsorption amount per unit of substrate area,  $n^{SV}$ , is given by

$$n^{SV}(x^V) = \sum_{\zeta=1}^{\zeta_{th}} \zeta a_\zeta(x^V), \quad (2)$$

where  $a_\zeta$  is the number of adsorbed clusters with  $\zeta$  molecules.

By using the canonical ensemble with  $\zeta$  cluster components and statistical thermodynamics, the canonical partition function of the adsorbate is obtained. By determining the Helmholtz function, the chemical potential expression for a cluster with  $\zeta$  molecules is obtained as<sup>20,32</sup>

$$\mu_\zeta^{SV} = k_B T^V \ln \left( \frac{a_\zeta}{a_0 q_\zeta} \right), \quad \text{for } \zeta = 1, 2, 3, \dots, \zeta_{th}, \quad (3)$$

where  $a_0$  is the number of unoccupied sites per unit area and  $q_\zeta$  is the partition function of a cluster with  $\zeta$  molecules and it is given by<sup>20,32</sup>

$$q_\zeta \equiv \left( \frac{\exp \left[ -\varepsilon_0^{(\zeta)} / (k_B T^V) \right]}{1 - \exp \left[ -\hbar \omega^{(\zeta)} / (k_B T^V) \right]} \right)^3. \quad (4)$$

In Eq. (4),  $\hbar$  is the reduced Planck constant and  $k_B$  is the Boltzmann constant. The power of three occurs because there are three degrees of freedom for the cluster. By approximating water vapor as an ideal gas, the chemical potential of vapor is expressed as

$$\mu^V(T^V, P) = \mu^V(T^V, P_{sat}(T^V)) + k_B T^V \ln \left( \frac{P}{P_{sat}} \right), \quad (5)$$

and by using the definition of  $x^V$ , the expression for Eq. (5) is simplified as

$$\mu^V(T^V, x^V) = \mu^V(T^V, P_{sat}(T^V)) + k_B T^V \ln(x^V). \quad (6)$$

If thermodynamic equilibrium exists between the adsorbate and the vapor, then it indicates that the chemical potential of a single-molecule cluster in the adsorbate and the chemical potential of vapor are equal,<sup>20,31</sup>

$$\mu_1^{SV}(T^V, x^V) = \mu^V(T^V, x^V), \quad (7)$$

and since the adsorbed phase is in local equilibrium,

$$\mu_1^{SV}(T^V, x^V) = \mu_\zeta^{SV}(T^V, x^V) / \zeta. \quad (8)$$

If there is equilibrium between the adsorbate and the vapor, then by using Eqs. (6)–(8), the chemical potential of the single-molecule cluster is given by

$$\mu_1^{SV}(T^V, x^V) = \mu_{sat}(T^V, P_{sat}) + k_B T^V \ln(x^V). \quad (9)$$

By using Eqs. (3), (7), and (9) and by defining two new nondimensional positive ZAI constants,  $c_{is}$  and  $\alpha$ , the fraction of adsorption sites that are occupied by a cluster with  $\zeta$  molecules,  $a_\zeta/M$ , can be expressed as follows:<sup>32,33</sup>

$$\frac{a_\zeta}{M} = \frac{c_{is}(\alpha x^V - 1)(\alpha x^V)^\zeta}{\alpha x^V [1 + c_{is}(\alpha x^V)^{\zeta_{th}} - c_{is}] - 1}, \quad \zeta = 1, 2, 3, \dots, \zeta_{th}. \quad (10)$$

Similarly, the fraction of empty adsorption sites,  $a_0/M$ , can be expressed as a function of the vapor pressure ratio,<sup>30–33</sup>

$$\frac{a_0}{M} = \frac{(\alpha x^V - 1)}{\alpha x^V [1 + c_{is}(\alpha x^V)^{\zeta_{th}} - c_{is}] - 1}. \quad (11)$$

Then, the number of molecules of adsorbate per unit area of the substrate at a given temperature, Eq. (2), is obtained by summing the expression  $\zeta a_\zeta(x^V)$  over all values of  $\zeta$  from 1 to  $\zeta_{th}$  and is given by<sup>30–33</sup>

$$n^{SV}(x^V) = \frac{M c_{is} \alpha x^V [1 - (1 + \zeta_{th})(\alpha x^V)^{\zeta_{th}} + \zeta_{th}(\alpha x^V)^{1+\zeta_{th}}]}{(1 - \alpha x^V)[1 + (c_{is} - 1)\alpha x^V - c_{is}(\alpha x^V)^{1+\zeta_{th}}]}. \quad (12)$$

The resulting thermodynamic adsorption isotherm is unique and confirms Gibbs's idea that the amount of vapor adsorbed per unit area at a given temperature is the same for all samples of a given material and independent of the surface area of the samples.<sup>31,34,35</sup> A detailed derivation of the ZAI by using quantum statistical thermodynamics is reported in earlier articles.<sup>20,31</sup>

It should be noted that the units of  $n^{SV}$  are number of molecules adsorbed per unit area. The ZAI constants  $c_{is}$ ,  $\alpha$ , and  $\zeta_{th}$  in Eq. (12) are nondimensional, whereas the remaining isotherm constant  $M$  is the number of adsorption sites per unit area. However, the experimental observations are normally recorded on a per-unit-mass basis of the substrate. Therefore, all area-specific relations are transformed into mass-specific relations by using the ZAI constant  $M_g$ , the number of adsorption sites per unit mass of substrate,

$$M_g = A_s M, \quad (13)$$

where  $A_s$  is the surface area per unit mass of substrate. By using Eqs. (10), (11), and (13), the cluster fractions are expressed on a per-unit-mass basis as

$$\frac{a_{\zeta_g}}{M_g} = \frac{c_{is}(\alpha x^V - 1)(\alpha x^V)^\zeta}{\alpha x^V [1 + c_{is}(\alpha x^V)^{\zeta_{th}} - c_{is}] - 1}, \quad \zeta = 1, 2, 3, \dots, \zeta_{th}, \quad (14)$$

and

$$\frac{a_{0g}}{M_g} = \frac{(\alpha x^V - 1)}{\alpha x^V [1 + c_{is}(\alpha x^V)^{\zeta_{th}} - c_{is}]}. \quad (15)$$

Similarly, by using Eqs. (12) and (13) the Zeta adsorption isotherm, the number of adsorbed molecules per unit mass of substrate, is expressed as

$$n_g^{SV}(x^V) = \frac{M_g c_{is} \alpha x^V [1 - (1 + \zeta_{th})(\alpha x^V)^{\zeta_{th}} + \zeta_{th}(\alpha x^V)^{1+\zeta_{th}}]}{(1 - \alpha x^V)[1 + (c_{is} - 1)\alpha x^V - c_{is}(\alpha x^V)^{1+\zeta_{th}}]}, \quad (16)$$

and this expression for  $n_g^{SV}$  is used to analyze the experimentally observed equilibrium adsorption amount in moles per unit mass. By performing a nonlinear regression analysis on the equilibrium data using the  $n_g^{SV}$  expression [Eq. (16)] as the model, all four ZAI constants ( $M_g$ ,  $c_{is}$ ,  $\alpha$ , and  $\zeta_{th}$ ) are determined, such that the normalized sum of squared residuals<sup>20,33</sup>  $Er$ ,

$$Er(n_g^{SV}, n_{exp}^{SV}) \equiv \frac{\sum_{i=1}^{N_i} (n_{exp}^{SV}(x_i^V) - n_g^{SV}(x_i^V))^2}{\sum_{i=1}^{N_i} n_{exp}^{SV}(x_i^V)}, \quad (17)$$

has a value less than 0.5%, where  $n_{exp}^{SV}(x_i^V)$  is the measured adsorption amount at a given pressure ratio,  $x_i^V$ , and  $n_g^{SV}(x_i^V)$  is the corresponding adsorption amount calculated using Eq. (16).  $N_i$  is the number of heterogeneity-free measured data points used in the regression.

The specific surface area of the adsorbent (i.e., surface area per unit mass of adsorbent) determined by the ZAI approach using water as an adsorbate,<sup>31</sup>  $A_s(\text{H}_2\text{O}, T)$ , is determined by knowing the cross-sectional area of an adsorbed water molecule at  $T$ ,  $\sigma(\text{H}_2\text{O}, T)$ , and is given by

$$A_s(\text{H}_2\text{O}, T) = M_g \sigma(\text{H}_2\text{O}, T), \quad (18)$$

where  $M_g$  is the number of adsorption sites per unit mass of the adsorbent determined from the equilibrium adsorption analysis. It is emphasized that if the experimental determination of  $n_g^{SV}$  is expressed as moles of adsorbate per unit mass, then the subsequent determination of the ZAI constant  $M_g$  is expressed as moles per

unit mass. In this case, the specific surface area of the substrate is obtained by

$$A_s(\text{H}_2\text{O}, T) = M_g \sigma(\text{H}_2\text{O}, T) N_A, \quad (19)$$

where  $N_A$  is Avogadro's number. The details of determining the thermodynamic isotherm of water vapor adsorbing on silica at 298 K from experimental observations were reported in an earlier article<sup>31</sup> and will be summarized in Sec. III.

### III. ZETA ADSORPTION ISOTHERM ANALYSIS OF WATER VAPOR ADSORPTION ON SILICA AT EQUILIBRIUM CONDITIONS

In a recent article,<sup>31</sup> the water-silica system at a temperature of 298 K was analyzed using data from four different silica samples. In that study, a comparative analysis of nitrogen and water vapor isotherms was done, and by using the ZAI, the area occupied by a water molecule,  $\sigma(\text{H}_2\text{O})$ , was obtained<sup>31</sup> to be 0.295 nm<sup>2</sup>. The validity of the determined value of  $\sigma(\text{H}_2\text{O})$  was then verified by transforming the mass-specific isotherms of four different fully hydroxylated silica samples<sup>28,31,36-38</sup> to area-specific isotherms by using their respective specific surface areas and when compared, they coincided on a single isotherm. This confirms Gibbs's idea of a thermodynamic isotherm.<sup>34</sup>

#### A. Heterogeneity-free equilibrium data

The ZAI approach for the adsorption of vapor on solid substrates assumes the adsorption to be heterogeneity-free. The reported mass-specific adsorption is said to be heterogeneity-free if the measured data satisfy the equilibrium condition and are thermodynamically phase-wise stable.<sup>33</sup> Heterogeneity-free data imply that the adsorption and desorption amounts at a given  $x^V$  are approximately the same within the experimental error bars. Furthermore, the effects of micropore filling<sup>39</sup> and capillary condensation<sup>26</sup> are assumed to be negligible in the heterogeneity-free range.

As described in earlier articles,<sup>32,33</sup> the heterogeneity-free data are identified by performing three successive nonlinear mass-specific regression analyses on the reported mass-specific water vapor adsorption data on a given silica sample. The first regression uses all the reported data and the ZAI expression, Eq. (16), as the model function to determine the four ZAI constants. By substituting the obtained constants ( $M_g$ ,  $c_{is}$ ,  $\alpha$ , and  $\zeta_{th}$ ) in Eq. (16), the calculated ZAI is determined and compared with the measured data. The measured data deviating from the calculated isotherm in the low pressure microporous heterogeneous range  $x^V \leq x_{\mu 2}^V$  and the upper higher pressure heterogeneous range  $x^V > x_m^V$  are visually identified

**TABLE I.** ZAI constants for water vapor adsorption on amorphous fully hydroxylated silica at 298 K. The error for the ZAI constants is the standard regression error. The results are reproduced from an earlier report.<sup>31</sup>

Solid powder	$T$ (K)	$\sigma_A$ (nm <sup>2</sup> )	$c_{is}$	$\alpha$	$\zeta_{th}$	$x_m^V$	$\alpha^{-1}$	$M$ ( $\mu\text{mol}/\text{m}^2$ )	$\gamma^{S0}$ ( $\text{mJ}/\text{m}^2$ )
Silica	298	0.295 $\pm 0.018$	8.8 $\pm 1.3$	0.97 $\pm 0.005$	78	0.9	1.031	5.63 $\pm 0.16$	163.2% $\pm 1\%$

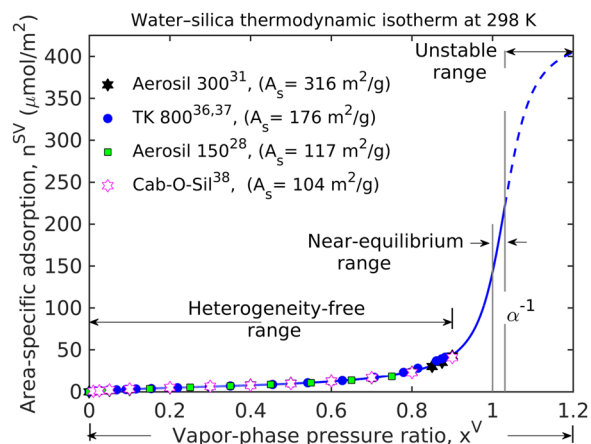


**FIG. 1.** Thermodynamic isotherm of water adsorbing on four fully hydroxylated silicas at 298 K.<sup>28,31,36–38</sup> The data points, indicated by the respective markers, are the area-specific adsorbed amounts from four different equilibrium adsorption datasets.<sup>31</sup> The solid line is the thermodynamic ZAI, calculated using Eq. (12) and the isotherm constants in Table I. The determined thermodynamic isotherm is extended beyond the equilibrium range to  $x^V \geq \alpha^{-1}$  and corresponds to the predicted adsorption value if the adsorption was to take place as heterogeneity-free.

and excluded in the second regression. Here,  $x_{\mu 2}^V$  and  $x_m^V$  are the lower and upper limits of the heterogeneity-free range. By using the determined constants, the stability of the adsorbate in the micropore range is examined by obtaining the molar latent heat, and then the low pressure micropore heterogeneity range  $x^V \leq x_{\mu 3}^V$  is finalized.

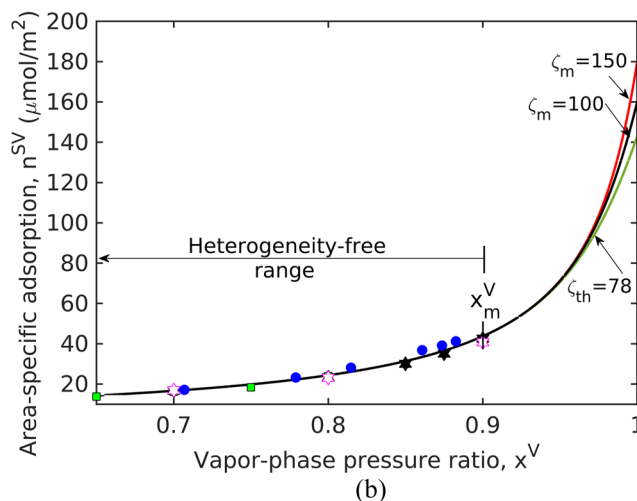
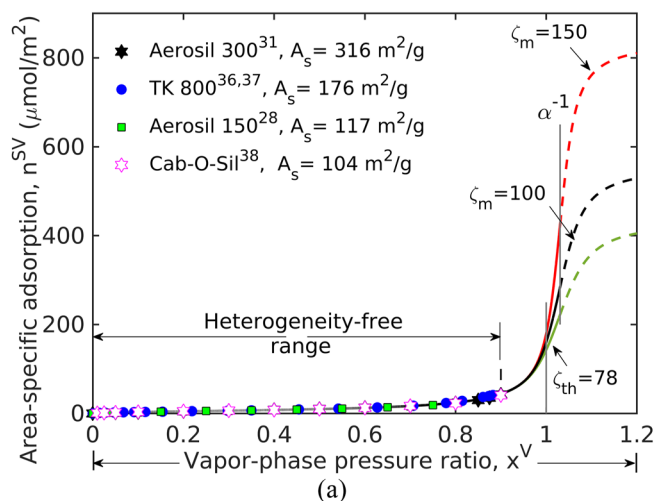


**FIG. 2.** The ZAI thermodynamic isotherms of water vapor adsorbing on silica are shown in (a) and are extended up to  $x^V$  equal  $\alpha^{-1}$ . The water vapor adsorbate is predicted to undergo a wetting transition at the interface when  $x^V$  approaches  $\alpha^{-1}$ . The effect of increasing the maximum cluster size beyond  $\zeta_{th}$  on the amount adsorbed is shown in (a). As seen in (b), the thermodynamic isotherm remains invariant with respect to  $\zeta$  greater than  $\zeta_{th}$  and diverges steeply in the near-equilibrium region as  $\zeta_m$  increases. (a) ZAI of water vapor adsorption on silica for three different maximum cluster sizes, up to thermodynamic limit,  $x_m^V$ .

The final regression in the heterogeneity-free range is performed and the ZAI constants are obtained.

## B. Thermodynamic isotherm of water vapor adsorption on silica

By using the number of moles of water vapor adsorption sites per gram of adsorbent,  $M_g$ , and the value of the cross-sectional area of an adsorbed water molecule on silica,  $\sigma_A(\text{H}_2\text{O})$ , in Eq. (19), the specific surface area,  $A_s$ , of a given sample was calculated. Similarly, the  $A_s$  of all the powdered silica samples currently used in this study were calculated and the details have been reported in an earlier article.<sup>31</sup> The mass-specific ZAIs of individual samples are then transformed to thermodynamic isotherms by using the respective specific surface areas of each sample. The thermodynamic isotherms of water vapor adsorbing on all four silica samples were obtained. The determined thermodynamic isotherms are seen to agree with the respective observed area-specific vapor adsorption data<sup>31</sup> of individual samples.

By pooling all four area-specific datasets of the silica samples to form a single dataset and then performing an area-specific non-linear regression analysis, the ZAI constants  $M$ ,  $c$ ,  $\alpha$ , and  $\zeta_{th}$  were obtained. All four ZAI constants, along with the upper limit of the heterogeneity-free range of the thermodynamic isotherm, which were earlier reported,<sup>31</sup> are listed in Table I. The threshold cluster size for water-silica is obtained such that it is the minimum value for which the values of  $M_g$ ,  $c_{is}$ ,  $\alpha$ , and  $n^{SV}$  in the range  $0 \leq x^V \leq 0.9$  are constant. The constants and calculated amount adsorbed,  $n^{SV}$ , remain invariant with any increase in cluster size greater than  $\zeta_{th}$ .

The determined thermodynamic isotherm shown in Fig. 1 is unique and independent of the specific surface areas of the samples and this supports the idea that the area-specific adsorption is

a property of the water–silica system at a given temperature.<sup>31,34,35</sup> Furthermore, in the plot it can be seen that the determined thermodynamic isotherm is extended for  $x^V$  values in the range  $x_m^V \leq x^V \leq 1$  and to the values in the near-equilibrium range. As  $x^V$  approaches  $\alpha^{-1}$ , the fraction of clusters of larger types increases, whereas the fraction of empty sites approaches zero and becomes negligible at  $\alpha^{-1}$ . Moreover, as  $x^V$  approaches  $\alpha^{-1}$  due the cluster interactions, a liquid-like film forms and condensation is initiated.<sup>24,33,40–43</sup> Using the adsorbate molar latent heat,  $\Lambda(x^V)$ , it was interpreted that, for  $x^V$  equal to  $\alpha^{-1}$ , the water vapor adsorbate undergoes a wetting transition. For values of  $x^V$  beyond  $\alpha^{-1}$ , the adsorbate is said to be in an unstable state.

As seen in Fig. 2(a), when the maximum cluster size is increased to  $\zeta_m$  such that it is greater than  $\zeta_{th}$ , the isotherm coincides with the thermodynamic isotherm drawn using  $\zeta_{th}$ , up to the upper heterogeneity limit,  $x_m^V$ , and then increases beyond the limit. Therefore, for any value of  $\zeta_m > \zeta_{th}$  the isotherms coincide up to  $x_m^V$  as shown in Fig. 2(b) and the predicted amount adsorbed increases steeply in the near-equilibrium region as  $\zeta_m$  increases [Fig. 2(a)].

The interpretation of the adsorbate in the near-equilibrium range of  $x^V$  values is based on the equilibrium thermodynamic isotherm and is not supported by any experimental data in that range. The extended thermodynamic isotherm and the wetting transition in the near-equilibrium range are therefore predictions. In this experimental study, we want to examine such a near-equilibrium prediction of the wetting transition by studying water vapor adsorption on a silica disk in order to analyze the stability of the adsorbate.

The near-equilibrium condition is initiated when the water vapor in contact with the substrate is saturated, the temperature of the water vapor is held constant at  $T^V$ , and the substrate surface acts as a heat sink by keeping its temperature  $T^S$  less than the vapor temperature,  $T^V$ . The ZAI approach assumes that, in the near-equilibrium state, the adsorbate is in local thermodynamic equilibrium.<sup>24</sup> In order to extend the ZAI into near-equilibrium conditions, we further assume that the ZAI and its constants listed in Table I are valid up to the wetting transition conditions.<sup>30</sup> The validity of these assumptions beyond the wetting point is not claimed as this range is unstable.

#### IV. ZETA ADSORPTION ISOTHERM AS A FUNCTION OF THE TEMPERATURE FUNCTION: NEAR-EQUILIBRIUM ANALYSIS

In the near-equilibrium region, the vapor-phase pressure ratio,  $x^V$ , cannot be used as the independent variable to perform experiments, even though valid theoretically, because it does not consider the temperature to which that the substrate is subcooled below the saturated vapor. Therefore, for the values of  $x^V$  in the range  $x^V > 1$ , a new dimensionless independent variable called the temperature function,  $y^{VS}$ , was defined,<sup>24,30</sup>

$$y^{VS} \equiv \left[ \frac{P_{sat}(T^V)}{P_{sat}(T^S)} \right]^{\frac{T^V}{T^S}} \quad \text{when } T^S < T^V, \quad (20)$$

where when  $y^{VS}$  becomes less than or equal to unity,  $T^S$  is equal  $T^V$ , then Eq. (20) becomes<sup>30</sup>

$$y^{VS} \equiv x^V \quad \text{for } 0 < y^{VS} \leq 1. \quad (21)$$

Equation (21) indicates that the respective definitions are identical in the thermal equilibrium range of  $0 < x^V \leq 1$ . Hence, the expression for the thermodynamic isotherm in the equilibrium region is the same expression as that of Eq. (12) with independent function variable  $x^V$  replaced with  $y^{VS}$ .

The temperature function acts as an extension of the pressure ratio in near-equilibrium conditions.<sup>24,30</sup> In the near-equilibrium condition, the value for the saturation pressure of the vapor,  $P_{sat}(T^V)$ , is nearly constant because  $T^V$  is maintained at a constant temperature. The substrate surface temperature, however, is progressively decreased below that of the vapor temperature, decreasing  $P_{sat}(T^S)$  and therefore increasing the value of  $y^{VS}$  above unity. The value for the saturation pressure at a given temperature for water is determined using the equation given by statistical rate theory.<sup>44</sup>

#### A. Chemical potential of the adsorbate and the ZAI in the near-equilibrium region

It should be noted that the cluster distribution expressions, Eqs. (10) and (11), and the ZAI expression, Eq. (12), given in Sec. II are expressed as functions of the relative vapor-phase pressure ratio,  $x^V$ . However, to perform experiments in the nonequilibrium range of  $x^V > 1$ , and analyze the adsorption data,  $x^V$  has to be replaced with the temperature function,  $y^{VS}$  [Eq. (20)] as an independent variable.

As mentioned above, the near-equilibrium region analysis is performed by subcooling the substrate at  $T^S$ , such that  $T^S < T^V$ . By using, Eq. (5), the chemical potential of vapor at a saturation pressure corresponding to the substrate temperature,  $T^S$ , is given as<sup>24</sup>

$$\mu^V(T^V, P_{sat}(T^S)) = \mu^V(T^V, P_{sat}(T^V)) + k_B T^V \ln \left( \frac{P_{sat}(T^S)}{P_{sat}(T^V)} \right). \quad (22)$$

Rewriting for chemical potential of vapor at the saturation pressure and vapor temperature,  $P_{sat}(T^V)$ , we have

$$\mu^V(T^V, P_{sat}(T^V)) = \mu^V(T^V, P_{sat}(T^S)) + k_B T^V \ln \left( \frac{P_{sat}(T^V)}{P_{sat}(T^S)} \right). \quad (23)$$

By using the definition of  $y^{VS}$ , Eq. (20), we have

$$\ln \left[ \frac{P_{sat}(T^V)}{P_{sat}(T^S)} \right] = \frac{T^S}{T^V} \ln y^{VS}. \quad (24)$$

Substituting Eq. (24) in Eq. (23), the chemical potential of vapor at  $P_{sat}(T^V)$  is

$$\mu^V(T^V, P_{sat}(T^V)) = \mu^V(T^V, P_{sat}(T^S)) + k_B T^S \ln [y^{VS}]. \quad (25)$$

Similar to the equilibrium analysis, the chemical potential of a single-molecule cluster of the adsorbate at near-equilibrium condition at  $T^S$  is in equilibrium with vapor, which is expressed as

$$\mu_1^{SV}(T^S) = \mu^V(T^V), \quad (26)$$

and since the adsorbed phase is in local equilibrium,

$$\mu_1^{SV}(T^S) = \mu_\zeta^{SV}(T^S)/\zeta = \mu^V(T^V). \quad (27)$$

Then, by using Eqs. (25)–(27), the chemical potential of the single-molecule cluster at  $T^S$  is given by

$$\mu_1^{SV}(T^S) = \mu^V(T^V, P_{sat}(T^S)) + k_B T^S \ln(y^{VS}). \quad (28)$$

As stated for the equilibrium analysis, by using the canonical ensemble with  $\zeta$  cluster components and statistical thermodynamics, the canonical partition function is obtained for the adsorbate in the near-equilibrium conditions. The chemical potential for a cluster with  $\zeta$  molecules at  $T^S$  is determined from the Helmholtz function of the adsorbate and is given as<sup>24</sup>

$$\mu_\zeta^{SV} = k_B T^S \ln\left(\frac{a_\zeta}{a_0 q_\zeta}\right), \quad \text{for } \zeta = 1, 2, 3, \dots, \zeta_m, \quad (29)$$

where  $q_\zeta$  is the partition function of a cluster with  $\zeta$  molecules and is given by<sup>24</sup>

$$q_\zeta \equiv \left( \frac{\exp\left[-\varepsilon_0^{(\zeta)} / (k_B T^S)\right]}{\left(1 - \exp\left[-\hbar\omega^{(\zeta)} / (k_B T^S)\right]\right)} \right)^\zeta. \quad (30)$$

The cluster fractions as a function of  $y^{VS}$  in the near-equilibrium conditions are obtained by using Eqs. (28) and (29) as<sup>23,24,31,33</sup>

$$\frac{a_\zeta}{M} = \frac{c_{istd} (\alpha_{td} y^{VS} - 1) (\alpha_{td} y^{VS})^\zeta}{\alpha_{td} y^{VS} [1 + c_{istd} (\alpha_{td} y^{VS})^{\zeta_m} - c_{istd}] - 1}, \quad \zeta = 1, 2, 3, \dots, \zeta_m \quad (31)$$

and

$$\frac{a_0}{M} = \frac{(\alpha_{td} y^{VS} - 1)}{\alpha_{td} y^{VS} [1 + c_{istd} (\alpha_{td} y^{VS})^{\zeta_m} - c_{istd}] - 1}. \quad (32)$$

Then, by using the expression  $a_\zeta(y^{VS})/M$  and summing the expression  $\zeta a_\zeta$  over all values of  $\zeta$  between 1 and  $\zeta_m$ , the ZAI expression for the near-equilibrium range is obtained as<sup>24,40</sup>

$$n^{SV}(y^{VS}) = \frac{M c_{istd} \alpha_{td} y^{VS} [1 - (1 + \zeta_m) (\alpha_{td} y^{VS})^{\zeta_m} + \zeta_m (\alpha_{td} y^{VS})^{1+\zeta_m}]}{(1 - \alpha_{td} y^{VS}) [1 + (c_{istd} - 1) \alpha_{td} y^{VS} - c_{istd} (\alpha_{td} y^{VS})^{1+\zeta_m}]}, \quad (33)$$

where the subscript *td* refers to thermal disequilibrium. It should be noted that similar definitions of the equilibrium ZAI constants were used here for thermal disequilibrium ZAI constants. However, as mentioned previously, the maximum cluster size,  $\zeta_m$ , is used instead of  $\zeta_{th}$ , and it is determined from a nonlinear regression analysis applied to combined equilibrium and disequilibrium data. The determined  $\zeta_m$  is usually such that  $\zeta_m \geq \zeta_{th}$ . It should be noted that the remaining equilibrium ZAI constants have been assumed to be approximately the same in the disequilibrium analysis<sup>24</sup> as in the equilibrium analysis by assuming that the adsorbate is in a local thermal equilibrium condition. Therefore, disequilibrium data are assumed to be approximately near-equilibrium data for the current analysis.

In the thermodynamic equilibrium limit, as stated by Eq. (21),  $y^{VS}$  equals  $x^V$  and therefore the area-specific isotherm  $n^{SV}(y^{VS}, \zeta_m)$  becomes the thermodynamic isotherm,  $n^{SV}(x^V, \zeta_m)$ ,

$$n^{SV}(y^{VS}, M, c_{is}, \alpha, \zeta_m) \rightarrow n^{SV}(x^V, M, c_{is}, \alpha, \zeta_m) \quad \text{for } 0 < x^V \leq 1. \quad (34)$$

Similarly, in the upper heterogeneity-free limit,  $x_m^V$ , the thermodynamic isotherm determined by using both equilibrium and nonequilibrium data,  $n^{SV}(y^{VS}, \zeta_m)$ , becomes equal to the equilibrium thermodynamic isotherm,  $n^{SV}(x^V)$ , obtained with threshold cluster size,  $\zeta_{th}$ ,

$$n^{SV}(y^{VS}, M, c_{is}, \alpha, \zeta_m) \rightarrow n^{SV}(x^V, M, c_{is}, \alpha, \zeta_m) = n^{SV}(x^V, M, c_{is}, \alpha, \zeta_{th}) \quad \text{for } 0 < x^V \leq x_m^V. \quad (35)$$

The equality of isotherms  $n^{SV}(x^V, \zeta_m)$  and  $n^{SV}(x^V, \zeta_{th})$  at the upper heterogeneity-free limit can be seen in Fig. 2(b). When nonequilibrium data are included, the isotherm  $n^{SV}(y^{VS}, \zeta_m)$  diverges in the range  $x^V > x_m^V$  and the following relation holds:

$$n^{SV}(y^{VS}, M, c_{is}, \alpha, \zeta_m) \rightarrow n^{SV}(x^V, M, c_{is}, \alpha, \zeta_m) \quad \text{for } 0 < y^{VS} < \alpha^{-1}, \quad (36)$$

where we have approximated the ZAI constants  $M$ ,  $c_{istd}$ , and  $\alpha_{td}$  for thermal disequilibrium analysis to be the same as the equilibrium ZAI constants.<sup>24</sup>

The determination of the thermodynamic isotherm as a function of  $y^{VS}$  by a nonlinear regression analysis on a pooled dataset of equilibrium and nonequilibrium data up to  $\alpha^{-1}$  is given in Sec. VI. The details of how the obtained isotherm is used in the stability analysis of the adsorbate and in the determination of solid surface energy of silica are presented in later sections (Secs. VII and VIII).

## V. EXPERIMENTAL INVESTIGATION OF NEAR-EQUILIBRIUM ADSORPTION CONDITIONS

In order to investigate the near-equilibrium adsorption properties and the subsequent phase transition of adsorbed water vapor on a fused silica substrate, an apparatus able to measure adsorbate film thickness at various values for the temperature function  $y^{VS}$  was created. A schematic diagram of the apparatus<sup>45</sup> is shown in Fig. 3. The thickness of the adsorbate film,  $\tau_m$ , was measured as a function of  $y^{VS}$  using a UV-visible interferometer (Filmetrics, USA). The error on the film thickness data was taken from the manufacturer's operating manual, i.e.,  $\pm 1$  nm. The error for the thermocouple measurements was  $\pm 0.02$  K.

### A. Materials and construction

The experimental apparatus, shown in Fig. 3, consisted of a stainless-steel evacuated chamber with four view-ports (Kurt J. Lesker, USA) and was designed to house a vertically oriented fused silica substrate of diameter 18 mm and thickness 10 mm (Technical Glass Products, USA). The surface of the fused silica substrate was polished to a surface roughness of 1 nm (Valleydesign, USA). The silica disk was mounted on a hollow stainless-steel cylinder, which was thermally maintained at the desired temperature by circulating refrigerant to the back of its surface (70% ethylene glycol, 30%

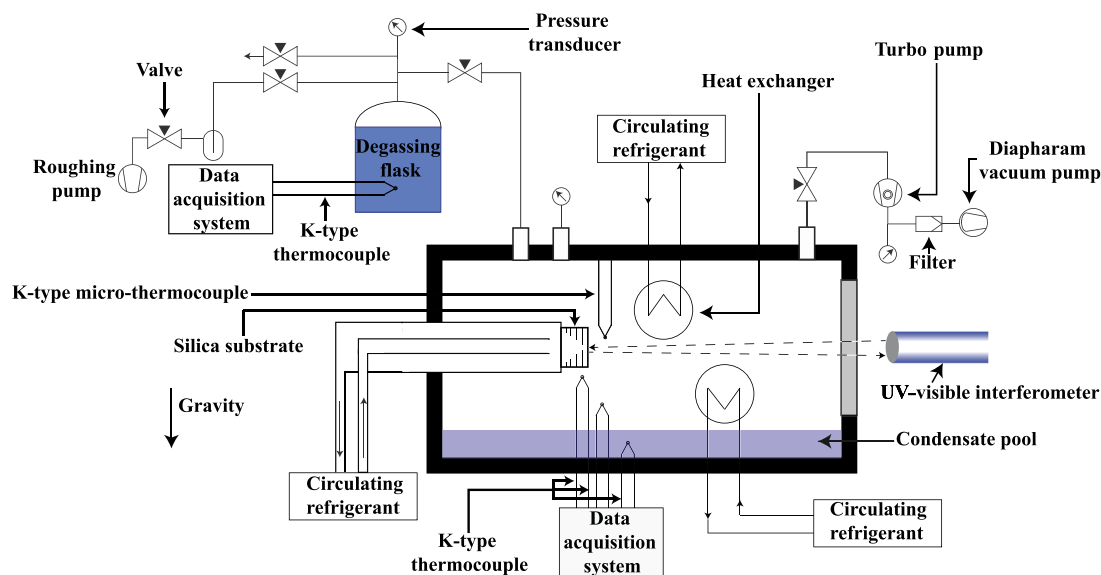


**FIG. 3.** Schematic of the experimental apparatus<sup>45</sup> used in this study. The apparatus was first evacuated to  $10^{-6}$  Pa and held at these conditions for over a week. A gas analyzer then confirmed the lack of contaminants in the chamber. The degassed water vapor was admitted to the chamber and was allowed to come to equilibrium. The back of the silica substrate was gradually cooled to bring the surface of the silica substrate to the desired temperature. Once the system had reached a steady state, the interferometer was used to measure the thickness of the adsorbate. The measurements at each of the  $\gamma^{\text{VS}}$  values are summarized in Table II.

deionized water). The silica disk was oriented such that it was perpendicular to the UV-visible interferometer's incident beam. The view-port between the interferometer and the disk was made out of a high-UV-transmittance quartz (Kurt J. Lesker, USA). The interferometer used a UV-visible light source and detector to measure film thickness to a resolution of 1 nm.

Sixteen thermocouple wells were drilled into the silica substrate disk at different radial, angular, and axial locations with varying depths. These thermocouple wells did not interact with the surface of the substrate and thus did not introduce any unintended nucleating sites for condensation. Sixteen nickel-chromium/nickel-aluminum (K-type) calibrated thermocouples ( $\pm 0.02$  K) were inserted in the wells and secured in place using thermally conductive epoxy [OB-101,  $k = 1.038$  W/(mK), Omega, USA].

Before the start of the study, all the chamber components were first rinsed with deionized, distilled, and nano-filtered water with a resistivity of  $18.17 \pm 0.1$  M $\Omega$  cm. The stainless-steel components of the chamber were initially rinsed with deionized water, acetone, and finally again with deionized water. The glassware components underwent an additional step of being rinsed with chromic-sulfuric acid (VWR, USA) before the final rinse with deionized water.<sup>45</sup>

In order to remove possible organic contaminants, which could influence the adsorption characteristics on the silica disk, a further cleaning procedure after the abovementioned acid and water treatment for each component was followed, to ensure a contamination-free experimental setup.<sup>45</sup> The chamber, which housed the silica disk, was first pumped down to reduce the pressure, using a mechanical pump (Welch DuoSeal, model number: 1402B-01). Subsequently, the chamber was connected to a roughing diaphragm vacuum pump (Edwards Rotary Vane Dual Stage Mechanical

Vacuum Pump) and a turbo-molecular pump (Leybold, UHV500) to create a high vacuum condition. The chamber was left for more than a week to ensure the removal of any contaminant vapor. Furthermore, before starting each experiment, the stainless-steel chamber walls were raised to a temperature of 200 for 48 h through electrical heating elements to speed up the release of contaminants and their subsequent removal by the vacuum pump. The absence of contaminants and the cleanliness of the vacuum chamber, maintained at  $10^{-6}$  Pa, were confirmed before each run using a residual gas analyzer (Stanford Research Systems, RGA 200, range up to 200 atomic mass units, USA), which showed no contaminants such as organic compounds in the mass spectrum of the experimental chamber.

## B. Experimental procedures

The water used in the experiments, as mentioned above, was distilled and deionized. It was then degassed in a clean glass flask while being stirred for 24 h. The degassing process was confirmed to be complete when the flask pressure was equal to the saturation pressure at the given temperature. The temperature of the chamber walls was reduced and maintained at a temperature below that of the saturated water vapor, and then the connection between the flask and chamber was opened. This resulted in the injected saturated water vapor condensing on the bottom of the chamber. The condensate pool ensured that the chamber's water vapor was always saturated. During the injection process, the silica disk's surface temperature was maintained above that of the injected saturated water vapor to reduce the amount adsorbed before the start of the experiment. This was confirmed by the interferometer showing the absence of any detectable adsorbate film on the surface of the silica. Then, the



connection between the chamber and the flask containing the water was closed, the chamber's temperature was raised to the desired temperature, and the chamber's pressure was measured to be that of the saturation pressure,  $P_{sat}(T^V)$ . The saturation pressure values were determined from the equation for the saturation pressure of water using statistical rate theory.<sup>44</sup>

The measurements from twelve out of the sixteen thermocouples embedded in the silica substrate were used to construct three boundary conditions for solving the axisymmetric, cylindrical, steady-state form of the heat equation.<sup>45,46</sup> The remaining four thermocouples of the silica substrate were used to test the accuracy of the solution to the heat equation.<sup>45</sup> The temperature field of the silica substrate was then extrapolated 1.5 mm to the surface of the silica, indicated<sup>45</sup> as  $T^S$ . Inside the chamber, we installed four calibrated ( $\pm 0.02$  K) K-type thermocouples, where one was a U-shaped micro-thermocouple with a bead diameter 38.4  $\mu\text{m}$  and the others had bead diameters of 270  $\mu\text{m}$ . The thermocouples were located at different heights in the chamber in order to measure the temperature gradient within the chamber. By using a network of heat exchangers inside the chamber, the temperature gradient was maintained to a negligible level such that it was below the error of the thermocouples. Thus, vapor temperature is assumed to be constant throughout the chamber for a given experiment.

### C. Experimental results

By using the experimental setup detailed in Sec. V B, experiments were conducted in the near-equilibrium range of water vapor adsorbing on a silica disk at 298 K. The results are listed in Table II. The measurements listed in Table II were made after steady-state conditions had been attained. Steady-state conditions were assumed when the experimental conditions were held for 2 h without any observable change in the measurements.

The water vapor film thicknesses,  $\tau_m$ , were measured for different  $y^{VS}$  values and were measured multiple times for each of the

experimental values of  $y^{VS}$ . The variance between the thickness readings did not exceed the reading accuracy of the system ( $\pm 1$  nm). Thirteen different experiments were conducted with the average vapor temperature ranging from 297.08 to 297.61 K.

For the same  $y^{VS}$ , as listed in Table II, multiple values of film thickness were measured, which supports the metastable nature of the adsorbed film at near-equilibrium conditions between saturation and wetting transition points. At saturation condition of  $x^V$  or  $y^{VS}$  equal to unity, the silica surface was measured to have an adsorbate film thickness of 2 nm. This value was assumed to represent the saturation condition since the temperature difference between the vapor and the substrate surface, i.e.,  $-0.02$  K, was within the error of the thermocouples. To obtain a value of  $y^{VS} > 1$ , the silica surface was cooled to a temperature below that of the adsorbing vapor, i.e., a positive subcooling value. To quantify the degree to which the substrate was subcooled, a variable  $\Delta T_{sub}$  is defined as

$$\Delta T_{sub} \equiv T^V - T^S, \quad (37)$$

where  $T^S$  is the substrate temperature.

Laboratory ambient conditions influenced water vapor temperature as the vapor temperature varied from experiment to experiment. The variations occurred despite good insulation and a network of heat exchangers, and as listed in Table II, we have a slight variation of water vapor temperature between experiments.

The increasing value of  $y^{VS}$  from unity indicates an increase in subcooling,  $T_{sub} > 0$ . The steps detailed above were repeated for each data point to ensure a steady-state measurement. No visible micron-sized droplets were present during the interferometer measurements, which would have indicated wetting had already occurred. The vapor temperature depended on the room temperature, so the vapor temperature was slightly different for each set of experiments; however, the vapor temperature was constant within each experimental run. The largest subcooling value achieved was

TABLE II. Water vapor adsorbate film thickness measurements in near-equilibrium conditions as a function of increasing subcooling temperature function.

Temperature function $y^{VS}$ $\pm 0.1$	Vapor temperature $T^V$ (K) $\pm 0.02$ K	Saturation vapor pressure <sup>44</sup> at $T^V$ , $P_s(T^V)$ (kPa) $\pm 1\%$	Substrate temperature $T^S$ (K) $\pm 0.02$ K	Saturation vapor pressure <sup>44</sup> at $T^S$ , $P_s(T^S)$ (kPa) $\pm 1\%$	Substrate subcooling $\Delta T_{sub}$ (K) $\pm 0.04$ K	Adsorbate film thickness $\tau_m$ (nm) $\pm 1$ nm	Adsorbed amount $n_r^{SV}$ ( $\mu\text{mol}/\text{m}^2$ ) $\pm 55 \mu\text{mol}/\text{m}^2$
1.0	297.56	3.0523	297.51	3.0432	0.05	5	276
1.01	297.53	3.0468	297.34	3.0127	0.19	5.2	287
1.01	297.56	3.0521	297.36	3.0151	0.2	7.7	428
1.01	297.5	3.0404	297.26	2.9981	0.23	9.1	502
0.999	297.61	3.0609	297.62	3.0640	-0.02	2.0	111
1.013	297.57	3.0536	297.35	3.0142	0.22	4.2	235
1.021	297.58	3.0552	297.23	2.9933	0.34	5.8	322
1.022	297.58	3.0558	297.22	2.9909	0.36	6.3	347
1.024	297.58	3.0552	297.19	2.9856	0.38	11.2	619
1.024	297.58	3.0559	297.19	2.9854	0.39	12.6	699
1.011	297.25	2.9962	297.06	2.9624	0.19	4.6	252
1.018	297.23	2.9929	296.94	2.9402	0.30	5.8	321
1.020	297.23	2.9927	296.90	2.9344	0.33	6.5	359

0.39 K, beyond which the steady-state conditions could not be maintained. This corresponds to a  $y^{VS}$  value of 1.024. Any attempt to increase  $y^{VS}$  by increasing the subcooling beyond this value resulted in droplet formation. This formation of droplets from the adsorbed film is thermodynamically an unsteady-state condition.

The average film thickness of the water vapor adsorbate was observed at the center of the vertically oriented silica disk using a UV-visible interferometer. There was no deviation of film thickness with respect to vertical distance for the disk. This indicates that the effect of gravity over the water vapor adsorbed film thickness on a polished silica disk is negligible. The measured adsorbate film thickness,  $\tau_m$ , was transformed into a number of moles adsorbed per unit area of the disk,  $n_r^{SV}$ , using

$$n_r^{SV}(y^{VS}) = \frac{\tau_m}{v_f(T^V)}, \quad (38)$$

where  $\tau_m$  is the measured average film thickness of the adsorbate on the silica substrate, and  $v_f(T^V)$  is the molar specific volume of the adsorbate calculated using the IAPWS-95 formulations.<sup>47</sup> Here, we assume that the molar specific volume of the adsorbate is equal to that of the saturated bulk liquid,  $v_f(T^V)$ .<sup>23,24,48</sup> The adsorbed amounts transformed from film thicknesses,  $\tau_m$ , in the near-equilibrium condition as a function of  $y^{VS}$  and the respective film thicknesses for all the experiments are shown in Table II. The error for the independent variable,  $y^{VS}$ , was calculated to be  $\pm 0.01$ , and the error<sup>49</sup> for the dependent variable,  $n^{SV}$ , was determined to be  $\pm 55 \mu\text{mol}/\text{m}^2$ .

## VI. ANALYSIS OF NEAR-EQUILIBRIUM CONDITIONS: ZETA ADSORPTION ISOTHERM APPROACH

The thermodynamic isotherm of the silica-water adsorption system at 298 K was determined using the ZAI constants  $M, c, \alpha$ , and  $\zeta_{th}$ , detailed in Table I. The obtained isotherm with a threshold cluster size,  $\zeta_{th}$ , of 78 is independent of the specific surface area of the silica samples. The determined thermodynamic isotherm predicted a finite amount of water vapor adsorption as  $x^V$  approaches unity. This is in contrast to the Brunauer-Emmett-Teller<sup>50</sup> (BET) approach, where the amount of adsorbate is predicted to be infinite as the saturation condition is approached. In the current study, we observed a finite amount of water vapor adsorption on silica in the near-equilibrium range before the wetting transition to a liquid phase at a value of  $x^V$  equal  $\alpha^{-1}$ .

Extending the independent variable from unity, replacing  $x^V$  with  $y^{VS}$ , we can plot the near-equilibrium data together with the equilibrium data from previous work.<sup>31</sup> As seen in Fig. 4, the thermodynamic isotherm with the previously determined ZAI constants does not describe the near-equilibrium data and predicts a lower adsorption amount at the respective values of  $y^{VS}$ . A new thermodynamic isotherm describing both equilibrium as well as near-equilibrium data can be determined by determining a new maximum number of adsorbate molecules in the cluster,<sup>40</sup>  $\zeta_m$ , such that it is greater than  $\zeta_{th}$ , and by assuming the other three ZAI constants to be same as in the equilibrium analysis. Therefore, by using Eq. (33) and performing a nonlinear regression on pooled equilibrium and near-equilibrium data as a single set, the maximum cluster

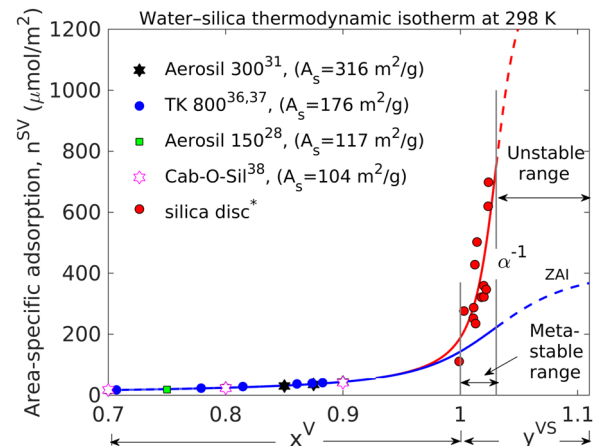


**FIG. 4.** Thermodynamic isotherm of the water-fully hydroxylated silica system for equilibrium and near-equilibrium regions. The red solid line is the determined thermodynamic isotherm using both equilibrium and near-equilibrium data and the maximum cluster size is 266. The solid blue line is the thermodynamic isotherm with a threshold cluster size of 78, obtained from equilibrium data of four different water-silica systems. The dashed lines are the extensions of the respective thermodynamic isotherms to the unstable region. The data for the silica disk are from the near-equilibrium experiment in this work.

size  $\zeta_m$  was obtained such that the normalized regression error, Eq. (17), was less than 0.05%.

As shown in Fig. 4, the new extended thermodynamic isotherm can be seen to agree well with equilibrium and near-equilibrium data points. The obtained maximum cluster size,  $\zeta_m$ , is  $266 \pm 17$ , where the error is the standard regression error for  $\zeta_m$ . As stated above in Eq. (17), the normalized regression error is obtained from the deviations between observed and calculated amounts and when this error is minimized to less than 0.5%, the standard regression error for  $\zeta_m$  is also minimized. The observed near-equilibrium data points are the adsorbed amounts obtained from the maximum film thicknesses that can be sustained and beyond that  $y^{VS}$ , the film could not be sustained. This indicates a metastable nature in the near-equilibrium range and this aspect of stability of the water vapor adsorbate is analyzed in detail in Sec. VI A.

### A. Initiation of dropwise condensation

The interferometer measurements for the independent experiments detailed in Table II indicate that the adsorbate film thickness increases in the near-equilibrium region of  $1 \leq y^{VS} \leq \alpha^{-1}$ . As seen in Table II, as  $y^{VS}$  was increased to 1.024, by subcooling the substrate up to 0.39 K, the film thickness reached an average maximum value of 12.6 nm. Beyond this value of  $y^{VS}$ , as shown in Fig. 5, the formation of visible droplets with an average diameter of  $30.90 \pm 12.14 \mu\text{m}$  was observed, indicating that the adsorbate is unstable and undergoes a phase transition to a liquid phase.

It should be noted that the interferometer readings were unreadable due to high noise, possibly due to micron-sized dropwise condensation, for  $y^{VS}$  values greater than 1.024. Beyond the wetting transition, we observed the formation of microdroplets, which grew and coalesced with adjacent droplets until they grew to a critical size after which they accelerated down sweeping other droplets along

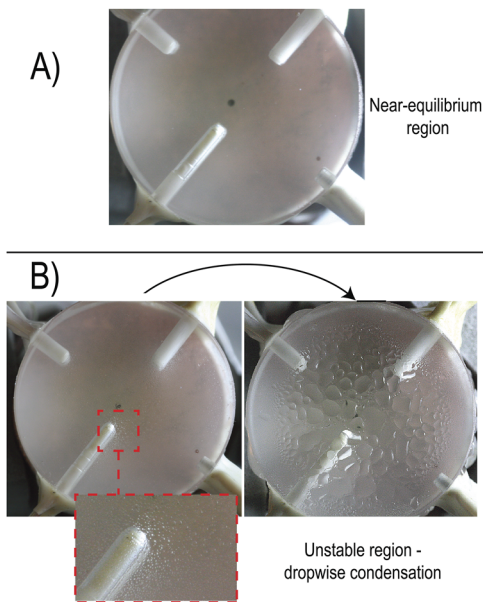


**FIG. 5.** The silica disk imaged using a high-zoom DSLR camera. The thermocouple wells have a white color due to the thermally conductive epoxy filling. The wells are drilled inside the silica and do not interfere with the surface. The black holes seen in the photographs are holes drilled into the copper backing and also did not interfere with the surface of the silica. (a) The surface of the silica disk in the near-equilibrium region. No visible micron-sized droplets, or larger, were seen to be present on the surface. (b) The behavior of the silica surface for  $y^{VS} > 1.024$ . Micron-sized droplets began to appear on the surface, with an average diameter of  $30.90 \pm 12.14 \mu\text{m}$ .

their way due to gravity. This cycle then restarted, much like what is expected of dropwise condensation.<sup>51</sup>

## VII. STABILITY OF THE WATER VAPOR ADSORBATE ON FUSED SILICA SURFACES

In Sec. III, we had shown the thermodynamic isotherm of water adsorbing on silica at 298 K, predicted from the equilibrium adsorption data from multiple datasets. The determined isotherm was then extended to above saturation conditions,  $1 < y^{VS} < \alpha^{-1}$ , and beyond. The ZAI thermodynamic isotherm in Fig. 4 can be seen to predict a finite amount adsorbed both at  $y^{VS}$  equal to unity and at  $y^{VS}$  equal to  $\alpha^{-1}$ . Furthermore, we have also stated that the thermodynamic isotherm is a property of the system and is independent of the specific surface area of the samples.<sup>31</sup> In order to determine the stability status of the adsorbate in the near-equilibrium region using the thermodynamic ZAI constants in Table I, the entropy of the adsorbate is determined. Using a canonical ensemble averaging, the entropy of the vapor adsorbing on the solid substrate,  $s^{SV}(y^{VS})$ , has been shown to be<sup>24,30,31</sup>

$$\frac{s^{SV}(y^{VS})}{k_B} = - \left[ \sum_{\zeta=0}^{\zeta_m} \left( \frac{a_\zeta(y^{VS})}{M} \ln \left( \frac{a_\zeta(y^{VS})}{M} \right) \right) \right], \quad (39)$$

where  $k_B$  is the Boltzmann constant and we have replaced  $x^V$  with  $y^{VS}$  for application to this work. Next, we proceed to calculate the heat of adsorption,  $q_H^{SV}$ , as a function of  $y^{VS}$ . It should be noted that the ZAI approach assumes that the vapor adsorbate on the substrate is constrained to be in an isothermal condition in the equilibrium and near-equilibrium range, i.e., we assume that the adsorbate is heated isothermally and quasi-statically by adsorption and kept at the vapor temperature by transferring this heat to the cooling reservoir (the copper backing with the flowing refrigerant). As per the first law of thermodynamics, a differential amount of heating,  $\delta q_H^{SV}$ , of the adsorbate by adsorption would increase the entropy of the adsorbate by a differential amount,  $ds^{SV}$ ,

$$\delta q_H^{SV} = T ds^{SV}. \quad (40)$$

The entropy expression of the water vapor adsorbate can be integrated to obtain the adsorbate heating due to the adsorption process,  $q_H^{SV}(y_r^{VS}, y^{VS})$ , where  $y_r^{VS}$  refers to an arbitrary state. After integrating Eq. (40), one obtains the expression for the adsorbate heating,  $q_H^{SV}(y_r^{VS}, y^{VS})$ ,

$$\begin{aligned} q_H^{SV}(y_r^{VS}, y^{VS}) &= T \int_{y_r^{VS}}^{y^{VS}} \left( \frac{\partial s^{SV}}{\partial y^{VS*}} \right) dy^{VS*}, \\ &= T [s^{SV}(y^{VS}) - s^{SV}(y_r^{VS})]. \end{aligned} \quad (41)$$

Since  $s^{SV}(0)$  is zero, and if  $N_0$  represents Avogadro's number, then the molar adsorbate heating may be written as

$$q_H^{SV}(0, y^{VS}) = -N_0 k_B T \sum_{\zeta=0}^{\zeta_m} \left( \frac{a_\zeta(y^{VS})}{M_g} \ln \left( \frac{a_\zeta(y^{VS})}{M_g} \right) \right). \quad (42)$$

The stability of the adsorbate can be analyzed by considering its molar latent heat,<sup>52</sup>  $\Lambda_a$ , defined<sup>31</sup> as

$$\Lambda_a = \frac{1}{N_0 k_B T} \left( \frac{\partial q_H^{SV}}{\partial y^{VS}} \right)_T. \quad (43)$$

As seen in Fig. 6, the latent heat is positive for the ranges,  $0 \leq x^V \leq 1$ , and  $1 < y^{VS} \leq \alpha^{-1}$ . The value of  $\Lambda_a$  is negative beyond  $y^{VS}$  equal  $\alpha^{-1}$ . As adsorption takes place, the adsorbate is heated and since the system is isothermal, the heat is removed by the cooling reservoir. If the latent heat is negative, it indicates that the adsorbate is cooled as the adsorption continues, which makes it unsustainable, and hence the adsorbate is interpreted to be in an unstable state.<sup>31,52</sup> It is observed in all experiments that with increase in the subcooling value, the film thickness also increases to a maximum thickness for the  $y^{VS}$  values that are shown in the plot. Further attempts to increase the subcooling value resulted in transition to the liquid phase. Due to instability, the adsorbate film is interpreted to have converted into droplets. However, all the experiments showed different maximum stable adsorbed amount at respective  $y^{VS}$  values beyond which stability could not be sustained. These experimental observations support the view that between  $y^{VS}$  equaling unity and  $\alpha^{-1}$ , the adsorbate is said to be in a metastable state.<sup>31</sup>

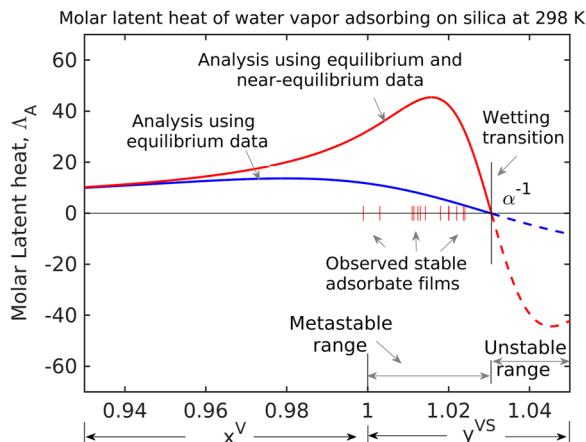


**FIG. 6.** Latent heat of adsorption,  $\Delta_a$ , as a function of  $x^V$  and  $y^{VS}$ , for the water–silica system. The solid red line represents  $\Delta_a$  predicted with  $\zeta_m$  and other thermodynamic isotherm constants listed in Table I. The solid blue line is  $\Delta_a$  predicted from equilibrium analysis. The figure also shows the  $y^{VS}$  values in the metastable range where the maximum film thicknesses were observed beyond which the film could not be sustained.

## VIII. SOLID SURFACE ENERGY OF THE SILICA SUBSTRATE

In an earlier article, the solid–vapor surface tension of water vapor adsorbing on silica nanopowder at 298 K was investigated using the ZAI<sup>31</sup> and the Gibbs adsorption equation,<sup>34</sup>

$$dy^{SV} = -n^{SV}(x^V) d\mu^{SV}. \quad (44)$$

By assuming water vapor to be an ideal gas, the chemical potential of the water vapor is<sup>28</sup>

$$\mu^V(T^V, x^V) = \mu_0^V(T^V, 1) + k_B T^V \ln(x^V), \quad (45)$$

where  $\mu_0$  is the reference chemical potential at saturation condition of  $x^V$  equal unity. By noting  $d\mu^{SV}$  equal  $d\mu^V$  at equilibrium and using Eq. (45) in Eq. (44), the Gibbs adsorption equation is expressed as

$$dy^{SV}(x^V) = -k_B T^V \frac{n^{SV}(x^V)}{x^V} dx^V. \quad (46)$$

It should be noted in the above expression that the amount adsorbed,  $n^{SV}$ , is expressed as number of molecules adsorbed per unit area. Using the ZAI thermodynamic isotherm, Eq. (12), and integrating, Eq. (46), from 0 to  $x^V$ , we have<sup>32,33</sup>

$$\gamma^{SV}(x^V, \zeta_{th}) = \gamma^{S0} - Mk_B T^V \ln \left( \frac{1 + (c_{is} - 1)\alpha x^V - c_{is}(\alpha x^V)^{\zeta_{th}+1}}{1 - \alpha x^V} \right), \quad (47)$$

where  $\gamma^{S0}$  is the solid surface energy of silica in the absence of adsorption and the ZAI constant  $M$  is expressed in units of number of adsorption sites per unit area. Therefore, as seen in Eq. (47), the solid–vapor interface energy,  $\gamma^{SV}$ , is a function of relative vapor pressure,  $x^V$ ,

$$\gamma^{SV} = \gamma^{SV}(\gamma^{S0}, M, c_{is}, \zeta_{th}, x^V), \quad (48)$$

where  $\gamma^{S0}$ ,  $M$ ,  $c_{is}$ , and  $\zeta_{th}$  are the constants of a given adsorption system. As  $x^V$  increases, the amount of adsorption on the substrate increases [Eq. (12)] and the solid–vapor energy of the substrate decreases from an initial value,  $\gamma^{S0}$ , at  $x^V$  equal 0,

$$\gamma^{SV} = \gamma^{S0} \quad \text{for } x^V = 0, \quad (49)$$

and the decrease in  $\gamma^{SV}$  with respect  $x^V$  is monotonic as will be shown later.

As stated in the previous articles<sup>23,24,30–33</sup> and in Sec. III, the adsorbate undergoes a wetting transition to liquid phase at  $x^V$  equal  $\alpha^{-1}$ . At this transition value of  $x^V$ , the solid–vapor interface energy,  $\gamma^{SV}$ , is assumed to be equal to that of the liquid–vapor interface energy,  $\gamma^{LV}$ . By using this boundary condition in Eq. (47), the solid surface energy of a silica substrate becomes<sup>33</sup>

$$\gamma^{S0} = \gamma^{LV} + \lim_{x^V \rightarrow \alpha^{-1}} \left[ Mk_B T^V \ln \left( \frac{1 + (c_{is} - 1)\alpha x^V - c_{is}(\alpha x^V)^{\zeta_{th}+1}}{1 - \alpha x^V} \right) \right]. \quad (50)$$

The value for  $\gamma^{S0}$  is found by assuming that the wetting transition occurs<sup>30,31</sup> as  $x^V$  reaches  $\alpha^{-1}$  and that  $\gamma^{SV}(\alpha^{-1})$  equals  $\gamma^{LV}$ . This wetting definition also assumes that the equilibrium contact angle in Young’s equation,  $\theta_e(\alpha^{-1})$ , becomes zero.<sup>28</sup> At the limiting condition of  $x^V$  approaching  $\alpha^{-1}$ , Eq. (50) simplifies to<sup>30–33</sup>

$$\gamma^{S0} = \gamma^{LV} + Mk_B T^V \ln(1 + c_{is}\zeta_{th}). \quad (51)$$

It should be noted that for values of  $x^V \geq 1$  in the near-equilibrium range, as stated earlier in Sec. IV, the temperature function,  $y^{VS}$ , is used as the independent variable. Moreover, as stated earlier, when the ZAI analysis was done on combined equilibrium and nonequilibrium data, the relation between  $n^{SV}(y^{VS})$  and  $n^{SV}(x^V)$  was given as

$$n^{SV}(y^{VS}, M, c_{is}, \alpha, \zeta_m) \rightarrow n^{SV}(x^V, M, c_{is}, \alpha, \zeta_m) \quad \text{for } 0 < y^{VS} < \alpha^{-1}, \quad (52)$$

where we have approximated the ZAI constants  $M$ ,  $c_{istd}$ ,  $\alpha_{id}$  for thermal disequilibrium analysis to be the same as those of the equilibrium ZAI constants.<sup>24</sup> Note that the ZAI adsorption isotherm,  $n^{SV}(x^V)$ , extended to the disequilibrium region with a maximum cluster size,  $\zeta_m$ , also describes the disequilibrium data. It may be recalled that  $n^{SV}(y^{VS}, \zeta_m)$  is identically similar to  $n^{SV}(x^V, \zeta_m)$ . This is not a surprise because  $n^{SV}(y^{VS}, \zeta_m)$  uses the same three equilibrium ZAI constants,  $(M, c_{is}, \alpha)$ , as an approximation.

It may be noted that the chemical potential of a single-molecule cluster when it is subcooled at  $T^S$  is expressed as a function of  $y^{VS}$  and it is given as Eq. (28),

$$\mu_1^{SV}(T^S) = \mu^V(T^V, P_{sat}(T^S)) + k_B T^S \ln(y^{VS}),$$

and therefore  $d\mu^{SV}$  is obtained as

$$d\mu_1^{SV} = k_B T^S \frac{dy^{VS}}{y^{VS}}. \quad (53)$$

By expressing the Gibbs adsorption equation as a function of  $y^{VS}$  as

$$d\gamma^{SV}(y^{VS}) = -n^{SV}(y^{VS})d\mu^{SV}(y^{VS}) \quad (54)$$

and substituting the expressions for  $d\mu^{SV}(y^{VS})$ , [Eq. (53)], in Eq. (54), we have

$$d\gamma^{SV}(y^{VS}) = -k_B T^S \frac{n^{SV}(y^{VS})}{y^{VS}} dy^{VS}. \quad (55)$$

By using the thermodynamic Zeta adsorption isotherm expression as a function of  $y^{VS}$ , Eq. (33), and integrating Eq. (55) from 0 to  $y^{VS}$ , the expression of  $\gamma^{SV}(y^{VS})$  is obtained as

$$\gamma^{SV}(y^{VS}, \zeta_m) = \gamma^{S0} - Mk_B T^S \ln \left( \frac{1 + (c_{is} - 1)\alpha y^{VS} - c_{is}(\alpha y^{VS})^{\zeta_m+1}}{1 - \alpha y^{VS}} \right), \quad (56)$$

where we have used maximum cluster size,  $\zeta_m$ , instead of the threshold cluster size  $\zeta_{th}$ .

Similarly, by using Eq. (56) and applying the boundary condition of  $\gamma^{SV}(\alpha^{-1})$  equals  $\gamma^{LV}$  as  $y^{VS}$  approaches  $\alpha^{-1}$ , the following expression for solid surface energy,  $\gamma^{S0}$ , is found:

$$\gamma^{S0} = \gamma^{LV} + Mk_B T^S \ln(1 + c_{is} \zeta_m). \quad (57)$$

As stated in Sec. IV A, the other three equilibrium ZAI constants  $M$ ,  $c_{is}$ , and  $\alpha$  are kept the same for the near-equilibrium analysis as in the equilibrium analysis. Moreover, it should be noted that the adsorbate is at a substrate temperature of  $T^S$  such that it is subcooled to a lower temperature than the vapor temperature  $T^V$ . Therefore, the vapor-adsorbate system is in a disequilibrium state. However, because the average subcooling value of all the experiments is 0.24 K, as stated in Sec. IV, we had approximated the disequilibrium observations as near-equilibrium states and proceeded with the ZAI analysis.

The value of the solid surface tension of fully hydroxylated silica in the absence of adsorption,  $\gamma^{S0}$ , was calculated to be  $163.2 \pm 1$  mJ/m<sup>2</sup> using the ZAI constants of the equilibrium data with Eq. (51), and it is a material property of fused hydroxylated silica. The surface tension of the solid-vapor interface,  $\gamma^{SV}$  or surface vapor interface energy, is a function of the amount adsorbed,  $n^{SV}(x^V)$ , on the interface.<sup>34</sup> As per the Gibbs adsorption equation, the surface tension of the solid decreases from its original value of  $\gamma^{S0}$  and reaches its minimum value at the wetting point.

If the solid surface energy of silica is calculated using the new maximum cluster size,  $\zeta_m$  in Eq. (57), we obtain a value of 180 mJ/m<sup>2</sup>, that is 12% more than that of the surface energy calculated from the equilibrium data. It should be noted that this analysis of calculating  $\gamma^{S0}$  using the vapor adsorption on the silica disk at a relative pressure ratio greater than unity is done by assuming local equilibrium approximations.<sup>23,24,28</sup>

As shown in Fig. 7, the respective plots of solid-vapor interface energy for the equilibrium and nonequilibrium analysis show a decrease in energy as  $x^V$  or  $y^{VS}$  increases. Moreover, as seen in Fig. 7, the maximum energy drop from no adsorption to the wetting transition is higher for the nonequilibrium experiment analysis when compared to the equilibrium analysis. Furthermore, both the plots also show that the surface energy drop is finite at  $x^V$  equal unity.

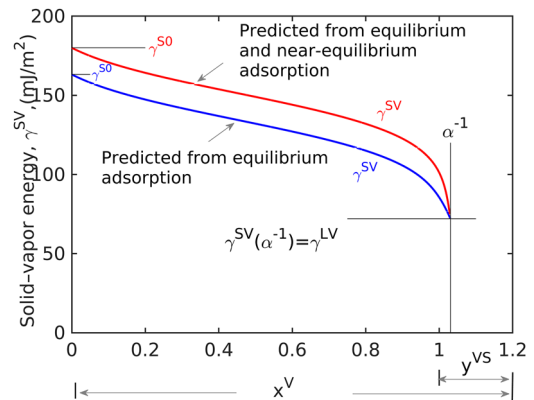


**FIG. 7.** Solid-vapor surface energy for the water-silica system. The solid red line representing  $\gamma^{SV}$  is predicted with both equilibrium and near-equilibrium data. It is plotted using Eq. (56) and the ZAI constants ( $M$ ,  $c_{is}$ ,  $\alpha$ , and  $\zeta_m$ ). The blue line is the plot of  $\gamma^{SV}$  for the water-silica system predicted from equilibrium data. This plot of decrease in surface vapor energy because of adsorption in the equilibrium range was done using Eq. (47) and the ZAI constants listed in Table I.

## IX. DISCUSSION

The objective of the current article was to examine the water vapor adsorption phenomena in the near-equilibrium region by an experimental procedure and then analyze the observations using ZAI analysis. Then, the results were compared with the predictions for the water-silica system from an equilibrium analysis.<sup>28,31</sup> In recently published articles<sup>23,24,40</sup> on experimental work in near-equilibrium conditions, a finite amount of organic vapor adsorption on a silicon substrate at saturation conditions and beyond was reported, and those findings supported the ZAI prediction from equilibrium analysis of organic vapor adsorption on silicon systems. In this study, we performed a similar experimental study and examined the water vapor adsorption on a silica disk up to the wetting transition of the adsorbate at 298 K. This study used the obtained thermodynamic isotherm for the water vapor-silica system<sup>31</sup> at 298 K by extending it to the near-equilibrium range and then tried to examine whether the adsorbate film thickness observations and the solid surface energy,  $\gamma^{S0}$ , calculated using these measurements, support each other.

In Sec. II, an overview of the ZAI<sup>20,32</sup> approach to the analysis of vapor adsorption on a nanopowder was given. By adopting the ZAI approach, the determination of the specific surface area of a silica nanopowder has been detailed where a value of 0.295 nm<sup>2</sup> for the occupied area of an adsorbed water molecule<sup>31</sup> is used at 298 K. Furthermore, by using the determined specific surface area of individual samples, the procedure for obtaining the thermodynamic isotherm,  $n^{SV}(x^V)$ , of the water vapor on a substrate and an expression for  $n^{SV}(x^V)$  was detailed in terms of the four ZAI constants.

In Sec. III, the use of the water vapor thermodynamic isotherm,  $n^{SV}$ , for the prediction of finite water vapor adsorption at  $x^V$  equal to unity and the adsorbate wetting transition point when  $x^V$  equals  $\alpha^{-1}$  were then detailed. The extension of  $n^{SV}$  to the near-equilibrium range was obtained from the analysis of equilibrium data up to an upper heterogeneity limit  $x_m^V$ . It should be noted that the prediction

of  $n^{SV}$  in the heterogeneous range of  $x^V$  between  $x_m^V$  and  $x^V \leq \alpha^{-1}$  indicating an amount adsorbed per unit area and the subsequent calculation of the solid surface energy of silica material are done by assuming the surfaces were free of heterogeneities. The ZAI constants ( $M$ ,  $c_{is}$ ,  $\alpha$ , and  $\zeta_{th}$ ) of the thermodynamic isotherm of water vapor adsorbing on silica were obtained by performing a nonlinear regression analysis on a pooled area-specific adsorption dataset from the adsorption data of four different silica nanopowders with varying specific surface areas.<sup>28,31,36–38</sup> The details of the regression results are given in Table I. It can be seen from Fig. 1 that the thermodynamic isotherm closely described all of the 65 data points and supports Gibbs's idea of area-specific adsorption at a given  $x^V$  as a system property.<sup>34</sup> It should be noted that the  $A_s$  values of all the silica samples were obtained using water vapor adsorption data with the ZAI approach. To experimentally verify this theoretical prediction in the near-equilibrium range of  $x^V \geq 1$ , the concept of the temperature function  $y^{VS}$  was detailed, and the resulting ZAI expression,  $n^{SV}$ , in terms of the temperature function was given as Eq. (33). By extending the thermodynamic isotherm to near-equilibrium conditions,  $y^{VS} \geq 1$ , the adsorbate wetting transition is predicted to occur at a temperature function of  $1.03 \pm 0.5\%$  and the plot of extended  $n^{SV}$  is shown in Fig. 1. The wetting transition predicted from the thermodynamic isotherm requires a subcooling value of 0.49 K at a vapor temperature of 298 K.

In this article, to examine the near-equilibrium prediction from equilibrium analysis with an experimental study, we used the film thickness measurements of water vapor adsorbing and then condensing on a nano-polished silica disk. The experiments were performed with an apparatus, as detailed in Sec. V, designed to operate with low-temperature measurement error of  $\pm 0.02$  K, which enabled us to investigate the near-equilibrium conditions in a small range of subcooling values. Experiments with a vapor temperature ranging from 297.23 to 297.61 K were conducted to examine the film growth due to adsorption and then the subsequent wetting transition in the near-equilibrium region. The adsorbate film thickness for each experiment was measured using a UV-visible interferometer and, as listed in Table II for each of the respective experiments, the film thickness grows as  $y^{VS}$  is increased up to the wetting transition point.

As detailed in Sec. V, the interferometer signals became incoherent and unreadable above a certain value of  $y^{VS}$ . We interpret this value of  $y^{VS}$  as the maximum  $y^{VS}$  at which the adsorbate was stable for the given experiment. When experiments were done to increase the film thickness further, the adsorbate transitioned to microdroplets and developed into dropwise condensation, as shown in Fig. 5. As detailed in Table II, the experimental, most stable observation for each of the experiments occurs at a lower subcooling value than the value of 0.49 K predicted from equilibrium analysis. From all the experiments, the steady-state, near-equilibrium adsorption observation was closest to the predicted wetting point (1.031) at a subcooling value of  $\sim 0.38$  K or a temperature function value of 1.024. Furthermore, the film thickness values vary from experiment to experiment for a given  $y^{VS}$ . The inability to obtain the same result in another experiment could be due to the sensitive nature of film thickness growth with  $y^{VS}$ .

By using Eq. (38), the adsorbate film thickness values from all the experiments are transformed to their respective adsorption

amount per unit area. Then, by including all the equilibrium and transformed near-equilibrium range of data, a nonlinear regression is performed to obtain a cluster size  $\zeta_m$  determined such that the determined  $n^{SV}$  nearly agrees with both ranges.

The obtained value of  $\zeta_m$  was  $266 \pm 17$  as compared with  $\zeta_{th}$  equal to 78 determined from equilibrium adsorption data alone. It should be noted that the other three Zeta isotherm constants  $M$ ,  $c_{is}$ , and  $\alpha$  were assumed to be the same for the two analyses. In this study, from the experiments performed, we have observed film thickness values that ranged from 2 to 5 nm near saturation condition of  $y^{VS}$  equal to unity and the equivalent amount adsorbed per unit area ranged from 111 to 276  $\mu\text{mol}/\text{m}^2$  by assuming the specific volume of the adsorbate to be the same as that of liquid water<sup>24</sup> at 298 K. The thermodynamic isotherm determined using all the equilibrium and near-equilibrium observations, as shown in Fig. 4, predicts at  $x^V$  equal to unity an adsorbed amount of 189  $\mu\text{mol}/\text{m}^2$  and it nearly agrees with the reported value of 139  $\mu\text{mol}/\text{m}^2$  from the equilibrium ZAI analysis. The equivalent film thicknesses were determined to be 3.41 and 2.51 nm for the near-equilibrium and equilibrium analyses, respectively.

Several investigators have attempted to analyze the film thickness growth due to water vapor adsorption on silica using ellipsometry<sup>53</sup> and spectroscopy.<sup>54</sup> In the work of Chibowski *et al.*,<sup>53</sup> using ellipsometry, a finite water vapor film thickness of 4.49 nm was reported as  $x^V$  approached unity at 298 K, whereas Assay and Kim using infrared spectroscopy reported a water vapor adsorbate film thickness of 2.76 nm at 290.15 K as  $x^V$  approached unity.<sup>54</sup> They had also observed that the adsorbed water near saturation consisted of distinct regions: one ice-like region near the solid surface where the silanols bond with the adsorbed water followed by a transitional layer followed by an adsorbed layer that is liquid-like.<sup>54</sup> In the work of Schlangen *et al.*,<sup>19,48</sup> it has been reported that water vapor adsorption approached a finite amount adsorbed on silica at near-saturation conditions and proposed that the adsorbate condenses as the vapor approaches supersaturation conditions. A similar finding was reported in the work of Wu *et al.*<sup>28</sup> using the ZAI approach for water adsorbing on silica at 298 K.

This study further supports the wetting transition of the adsorbate film to a liquid state on the interface prior to a dropwise condensation. We observed that the liquid condensate is present all over the substrate with no visible bias for sites with different gravitational potential. This phenomenon was also observed with the interferometer in the near-equilibrium region,  $1 < y^{VS} \leq 1.02$ , in that there was no difference in the thickness of the adsorbate film as the interferometer's beam changed between locations of differing gravitational potential on the surface of the substrate. This observation can be contrasted with a similar ZAI analysis done for heptane adsorbing on a silicon substrate,<sup>23,24</sup> which showed the amount adsorbed being a function of gravitational potential energy. One possible interpretation for this difference in results is that for the water-silica system, the metastable range in the near-equilibrium region is much narrower than that of the heptane-silicon system. The current metastability range for the water vapor-silica system is  $1 < y^{VS} \leq 1.024$ , whereas for the heptane-silicon system it is  $1 < y^{VS} \leq 1.17$ . Moreover, for the water-silica system, the measured film thicknesses are quite small and the spatial variability of adsorbed film thickness due to gravity could be below the detection limit of the interferometer.

The metastability of the water vapor adsorbate in the near-equilibrium region of  $y^{SV}$  up to  $\alpha^{-1}$  and the subsequent unstable nature of the adsorbate after transitioning to liquid phase is discussed in Sec. VII. As shown in Fig. 6, the adsorbate latent heat changes sign from positive to negative at  $y^{VS}$  equal  $\alpha^{-1}$ . The negative latent heat beyond  $\alpha^{-1}$  is interpreted as indicating the unstable nature of the adsorbate and the ZAI analysis in this range of  $y^{VS}$  is no longer valid because the adsorbate has transitioned to another phase. All the experiments showed different maximum stable adsorbed amount at their respective  $y^{VS}$  values beyond which stability could not be sustained. Furthermore, the same experimental observation could not be repeated between experiments. All these experimental observations support the metastable nature<sup>31</sup> of the adsorbate in the range  $1 \leq y^{VS} \leq \alpha^{-1}$ .

In this experiment, we assumed that both the amorphous silica, whose thermodynamic isotherm is extended to predict the wetting transition, and the planar glass surface on which the vapor condensation was performed, are fully hydroxylated and have similar surface silanol concentrations. Based on the thermodynamic isotherm at 298 K, the concentration of surface silanol groups for the hydroxylated silica is reported<sup>31</sup> as 3.39 silanols per  $\text{nm}^2$  (Table I), with a one-to-one correspondence between the adsorbed water molecule and the silanols in the interface.<sup>31,55</sup> A higher value of silanol concentration has been reported by various investigations<sup>36,56,57</sup> using the BET<sup>50</sup> area. These silanol groups, which have been classified as isolated, geminal, and vicinal using infrared spectroscopy and other techniques,<sup>57</sup> have distinct hydrogen bonding properties with the water adsorbate. These silanol groups at the saturated concentration on the silica disk enabled a wettable condition for the silica disk. It has been reported that these silanols give rise to different silica surface–water adsorbate, adsorbate–adsorbate, and adsorbate–vapor structural regions.<sup>57</sup> The current variation of stable film thickness between 1 and 9 nm could be due to the initial distribution of various silanol groups in the disequilibrium range. Such a large variation of film thickness near saturation has also been reported by various authors.<sup>58–60</sup> The observed variation in film thickness in the near-equilibrium range could also be due to the averaging technique used in the interferometer to measure film thickness and the adsorbed film having various sized clusters before transitioning to a wetting film at  $\alpha^{-1}$ .

Furthermore, it is known that contamination of the silica disk is a factor in the adsorbate thickness. Possible contamination could perturb the interacting fields<sup>58</sup> between the substrate and the adsorbate. Any long running experiment could result in a contaminated system and, because surface properties of high energy surfaces such as silica are very sensitive to contamination, the film thickness could be influenced, perturbing the system to form microdroplets.<sup>58,61–63</sup> To reduce the impact of contaminants, as mentioned in Sec. V, the system was baked at a high temperature and then evacuated to a vacuum pressure of  $10^{-6}$  Pa before introducing water vapor to the experimental section.<sup>45</sup>

The unstable nature of film thickness after the transition is marked by a dropwise condensation at large subcooling values and its interpretation is beyond the scope of this paper. We also make no conclusion about whether submicron droplets exist or not in the near-equilibrium region where the adsorbed film was observed. The film thickness measurements were an average thickness that existed on the silica substrate and one can assume that submicron droplets

could indeed reside on the surface of the silica around the adsorbate film. If such submicron droplets did exist in the metastable region, they did not have a significant effect on the operation of the UV–visible interferometer since negligible noise was measured by the UV–visible interferometer until the unstable region was reached. In 1957, Derjaguin and Zorin,<sup>59</sup> in their work studying the adsorption of supersaturated vapor of a polar substance (such as water) on a “carefully cleaned glass plate,” found that at supersaturation conditions, nucleating droplets coexisted alongside the adsorbed film.<sup>59,64</sup> Grant and Salthouse later backed up this theory by studying surface resistivity of thin adsorbed films.<sup>64</sup> In 1936, Jacob suggested condensation begins initially as a film and at a certain critical film thickness, the film becomes hydrodynamically unstable and ruptures into multiple droplets.<sup>65</sup> This idea was later discussed by Majumdar and Mezić.<sup>66</sup> We are unable to conclude between film rupture or nucleation; this is especially because measurements of film thickness (or lack thereof) are not possible after micron-sized droplets form on the surface of the substrate above the near-equilibrium region. It is shown here that a nano-thin film resides on the silica surface and it grows as a function of subcooling value starting from saturation and ambient temperature conditions before dropwise condensation takes place.

In Sec. VI, we analyzed the variation of the solid–vapor surface energy as a function of  $x^V$  for equilibrium and as a function of  $y^{VS}$  for the near-equilibrium range for the water–silica system. As seen in Fig. 7, the solid–vapor energy,  $\gamma^{SV}$ , drops as the adsorption pressure ratio increases due to the adsorption of water vapor for both equilibrium and near-equilibrium analyses. At  $y^{VS}$  equals  $\alpha^{-1}$ ,  $\gamma^{SV}$  equals  $\gamma^{LV}$  and the adsorbate is interpreted to transition to a liquid phase. The current experimental observation supports the predicted value of the wetting transition value of  $\alpha^{-1}$  because all stable film thicknesses occurred at  $y^{VS}$  values less than  $\alpha^{-1}$ . The surface energy drop at saturation condition of  $x^V$  equal to unity is shown to be finite from both the equilibrium and near-equilibrium analyses unlike the infinite energy drop predicted by BET theory.<sup>67–70</sup>

The finite amount adsorbed for saturated conditions and in the near-equilibrium range supports the prediction from the thermodynamic isotherm of water on a fully hydroxylated silica surface by the Zeta adsorption isotherm approach. This is in contrast to the BET isotherm, which does not describe experimental adsorption data beyond  $x^V > 0.35$  and diverges to infinity as  $x^V$  approaches unity.<sup>61</sup> It also supports the findings of water vapor film metastability detailed in the work of Schlangen *et al.*<sup>19</sup> This study further closely supports the prediction of equilibrium analysis of the wetting transition point and the solid surface energy of silica, which is a material property at a given temperature.

## X. CONCLUSION

This study gives insight into the transition from an equilibrium adsorbed film to the nucleation of condensed droplets. The water vapor’s adsorption and wetting characteristics on a nanopolished hydroxylated silica disk were examined and compared with the prediction from the ZAI equilibrium analysis. An overview of the ZAI approach and the determination of the thermodynamic isotherm were detailed for the water–silica system at 298 K. Using the extended thermodynamic isotherm and latent heat analysis,

wetting transition characteristics were predicted at  $y^{VS}$  equal to  $\alpha^{-1}$ . The near-equilibrium experiments were performed using a UV-visible interferometer, which measured the adsorbate film thickness at varying subcooling conditions for a vertically oriented silica disk in contact with saturated water vapor. Different experiments were conducted, which showed a maximum stable film thickness occurred for values of the temperature function,  $y^{VS}$ , ranging from 1.0 to 1.024. All these observations were less than the predicted transition point ( $y^{VS}$  equal 1.031).

By performing a nonlinear regression analysis on pooled equilibrium and near-equilibrium observations, the maximum cluster size  $\zeta_m$  was determined to be  $266 \pm 17$  compared to threshold cluster size  $\zeta_{th}$  of 78 when only equilibrium data were included in the regression. The thermodynamic isotherm obtained equilibrium ZAI constants,  $M$ ,  $c_{is}$ ,  $\alpha$ , with maximum cluster size,  $\zeta_m$ , nearly describe all the equilibrium and near-equilibrium data observations. The surface energy decreases as a function of  $x^V$  in the equilibrium range and as a function  $y^{VS}$  in the near-equilibrium conditions up to the wetting transition of  $y^{VS}$  equal to  $\alpha^{-1}$  were calculated. The energy decrease due to adsorption was calculated to be higher than that predicted from the equilibrium analysis. The difference between the predicted and the observed wetting characteristics in the near-equilibrium conditions suggests a metastable nature of the adsorption in that region.

The experimental studies showed that beyond the wetting point, the adsorbate transitioned into visible micron-sized droplets, which supports the ZAI prediction that the adsorbate becomes thermodynamically unstable. The presence of adsorbed molecules along with the droplets in the unstable region cannot be analyzed because the ZAI assumptions are no longer valid in this unstable region due to the nonequilibrium nature of the adsorbate.

## ACKNOWLEDGMENTS

The authors gratefully acknowledge the support received from the Natural Sciences and Engineering Research Council of Canada, the Canadian Space Agency, and the European Space Agency. J. A. W. Elliott holds a Canada Research Chair in Thermodynamics.

## AUTHOR DECLARATIONS

### Conflict of Interest

The authors have no conflicts to disclose.

### Author Contributions

Sepehr Saber and Nagarajan Narayanaswamy have contributed equally to experimental, analysis, and manuscript efforts. C. A. Ward directed and supervised this work until his death on October 12, 2022. After C. A. Ward's passing, Janet A. W. Elliott contributed significantly to the analysis, direction, and editing of the work.

**Sepehr Saber:** Conceptualization (equal); Data curation (equal); Formal analysis (equal); Investigation (equal); Methodology (equal); Validation (equal); Visualization (equal); Writing – original draft (equal); Writing – review & editing (equal). **Nagarajan**

**Narayanaswamy:** Conceptualization (equal); Formal analysis (equal); Investigation (equal); Methodology (equal); Software (equal); Validation (equal); Visualization (equal); Writing – original draft (equal); Writing – review & editing (equal). **C. A. Ward:** Conceptualization (equal); Formal analysis (equal); Funding acquisition (equal); Investigation (equal); Methodology (equal); Project administration (equal); Resources (equal); Supervision (equal); Validation (equal); Visualization (equal). **Janet A. W. Elliott:** Formal analysis (equal); Methodology (equal); Supervision (equal); Visualization (equal); Writing – review & editing (equal).

## DATA AVAILABILITY

The data that support the findings of this study are available within the article.

## REFERENCES

- 1 A. Verdager, G. M. Sacha, H. Bluhm, and M. Salmeron, "Molecular structure of water at interfaces: Wetting at the nanometer scale," *Chem. Rev.* **106**, 1478–1510 (2006).
- 2 A. L. Barnette, D. B. Asay, and S. H. Kim, "Average molecular orientations in the adsorbed water layers on silicon oxide in ambient conditions," *Phys. Chem. Chem. Phys.* **10**, 4981–4986 (2008).
- 3 S. Romero-Vargas Castrillón, N. Giovambattista, I. A. Aksay, and P. G. Debenedetti, "Structure and energetics of thin film water," *J. Phys. Chem. C* **115**, 4624–4635 (2011).
- 4 E. Papirer, *Adsorption on Silica Surfaces* (CRC Press, 2000), Vol. 90.
- 5 F. H. Cocks, P. A. Klenk, S. A. Watkins, W. N. Simmons, J. C. Cocks, E. E. Cocks, and J. C. Sussingham, "Lunar ice: Adsorbed water on subsurface polar dust," *Icarus* **160**, 386–397 (2002).
- 6 A. Abdelmonem, S. Ratnayake, J. D. Toner, and J. Lützenkirchen, "Cloud history can change water-ice-surface interactions of oxide mineral aerosols: A case study on silica," *Atmos. Chem. Phys.* **20**, 1075–1087 (2020).
- 7 T. J. Dening, D. Zemlyanov, and L. S. Taylor, "Application of an adsorption isotherm to explain incomplete drug release from ordered mesoporous silica materials under supersaturating conditions," *J. Controlled Release* **307**, 186–199 (2019).
- 8 J. Frelichowska, M.-A. Bolzinger, and Y. Chevalier, "Pickering emulsions with bare silica," *Colloids Surf., A* **343**, 70–74 (2009).
- 9 R. H. Mohammed, O. Mesalhy, M. L. Elsayed, S. Hou, M. Su, and L. C. Chow, "Physical properties and adsorption kinetics of silica-gel/water for adsorption chillers," *Appl. Therm. Eng.* **137**, 368–376 (2018).
- 10 M. Salman, S. Jahan, S. Kanwal, and F. Mansoor, "Recent advances in the application of silica nanostructures for highly improved water treatment: A review," *Environ. Sci. Pollut. Res.* **26**, 21065–21084 (2019).
- 11 D. Wang, J. Zhang, X. Tian, D. Liu, and K. Sumathy, "Progress in silica gel-water adsorption refrigeration technology," *Renewable Sustainable Energy Rev.* **30**, 85–104 (2014).
- 12 A. Kumar, C. Marcolli, and T. Peter, "Ice nucleation activity of silicates and aluminosilicates in pure water and aqueous solutions—Part 2: Quartz and amorphous silica," *Atmos. Chem. Phys.* **19**, 6035–6058 (2019).
- 13 J. M. Rosenholm and M. Lindén, "Towards establishing structure–activity relationships for mesoporous silica in drug delivery applications," *J. Controlled Release* **128**, 157–164 (2008).
- 14 J. Frelichowska, M.-A. Bolzinger, and Y. Chevalier, "Effects of solid particle content on properties of o/w Pickering emulsions," *J. Colloid Interface Sci.* **351**, 348–356 (2010).
- 15 D. Napierska, L. C. J. Thomassen, D. Lison, J. A. Martens, and P. H. Hoet, "The nanosilica hazard: Another variable entity," *Part. Fibre Toxicol.* **7**, 39 (2010).
- 16 S. J. Gregg and K. S. W. Sing, *Adsorption, Surface Area, and Porosity* (Academic Press, 1982).



- <sup>17</sup>S. Maier and M. Salmeron, "How does water wet a surface?," *Acc. Chem. Res.* **48**, 2783–2790 (2015).
- <sup>18</sup>S. Yamamoto, K. Andersson, H. Bluhm, G. Ketteler, D. E. Starr, T. Schiros, H. Ogasawara, L. G. M. Pettersson, M. Salmeron, and A. Nilsson, "Hydroxyl-induced wetting of metals by water at near-ambient conditions," *J. Phys. Chem. C* **111**, 7848–7850 (2007).
- <sup>19</sup>L. J. M. Schlangen, L. K. Koopal, M. A. Cohen Stuart, and J. Lyklema, "Wettability: Thermodynamic relationships between vapour adsorption and wetting," *Colloids Surf., A* **89**, 157–167 (1994).
- <sup>20</sup>C. A. Ward and J. Wu, "Effect of adsorption on the surface tensions of solid–fluid interfaces," *J. Phys. Chem. B* **111**, 3685–3694 (2007).
- <sup>21</sup>H. Ghasemi and C. A. Ward, "Surface tension of solids in the absence of adsorption," *J. Phys. Chem. B* **113**, 12632–12634 (2009).
- <sup>22</sup>C. A. Ward and K. Sefiane, "Adsorption at the solid–liquid interface as the source of contact angle dependence on the curvature of the three-phase line," *Adv. Colloid Interface Sci.* **161**, 171–180 (2010).
- <sup>23</sup>S. Yaghoubian and C. A. Ward, "Initiation of wetting, filmwise condensation and condensate drainage from a surface in a gravity field," *Phys. Chem. Chem. Phys.* **19**, 20808 (2017).
- <sup>24</sup>S. Yaghoubian, S. H. Zandavi, and C. A. Ward, "From adsorption to condensation: The role of adsorbed molecular clusters," *Phys. Chem. Chem. Phys.* **18**, 21481 (2016).
- <sup>25</sup>S. H. Zandavi and C. A. Ward, "Vapour adsorption kinetics: Statistical rate theory and zeta adsorption isotherm approach," *Phys. Chem. Chem. Phys.* **18**, 25538–25545 (2016).
- <sup>26</sup>S. H. Zandavi and C. A. Ward, "Nucleation and growth of condensate in nanoporous materials," *Phys. Chem. Chem. Phys.* **17**, 9828–9834 (2015).
- <sup>27</sup>S. H. Zandavi and C. A. Ward, "Characterization of the pore structure and surface properties of shale using the zeta adsorption isotherm approach," *Energy Fuels* **29**, 3004–3010 (2015).
- <sup>28</sup>C. Wu, S. H. Zandavi, and C. A. Ward, "Prediction of the wetting condition from the zeta adsorption isotherm," *Phys. Chem. Chem. Phys.* **16**, 25564–25572 (2014).
- <sup>29</sup>S. H. Zandavi and C. A. Ward, "Clusters in the adsorbates of vapours and gases: Zeta isotherm approach," *Phys. Chem. Chem. Phys.* **16**, 10979–10989 (2014).
- <sup>30</sup>N. Narayanaswamy and C. A. Ward, "Specific surface area, wetting, and surface tension of materials from N<sub>2</sub> vapor adsorption isotherms," *J. Phys. Chem. C* **123**, 18336–18346 (2019).
- <sup>31</sup>N. Narayanaswamy and C. A. Ward, "Area occupied by a water molecule adsorbed on silica at 298 K: Zeta adsorption isotherm approach," *J. Phys. Chem. C* **124**, 9269–9280 (2020).
- <sup>32</sup>N. Narayanaswamy and C. A. Ward, "Thermodynamic N<sub>2</sub> vapor isotherms of materials: Zeta adsorption isotherm approach," *J. Phys. Chem. C* **125**, 8440–8455 (2021).
- <sup>33</sup>N. Narayanaswamy and C. A. Ward, "Specific surface area of nanopowders from argon adsorption at 77 and 87 K: Zeta adsorption isotherm approach," *J. Phys. Chem. C* **125**, 28115–28135 (2021).
- <sup>34</sup>J. W. Gibbs, "On the equilibrium of heterogeneous substances," in *The Scientific Papers of J. Willard Gibbs* (Dover, New York, 1961), Vol. 1, pp. 55–349.
- <sup>35</sup>J. A. W. Elliott, "Gibbsian surface thermodynamics," *J. Phys. Chem. B* **124**, 10859–10878 (2020).
- <sup>36</sup>F. S. Baker, "Adsorptive properties of chromium oxides and silica," Ph.D. thesis, Brunel University, 1974.
- <sup>37</sup>F. S. Baker and K. S. W. Sing, "Specificity in the adsorption of nitrogen and water on hydroxylated and dehydroxylated silicas," *J. Colloid Interface Sci.* **55**, 605 (1975).
- <sup>38</sup>R. L. Every, W. H. Wade, and N. Hackerman, "Free energy of adsorption. I. The influence of substrate structure in SiO<sub>2</sub>–H<sub>2</sub>O, SiO<sub>2</sub>–n-Hexane and SiO<sub>2</sub>–CH<sub>3</sub>OH systems," *J. Phys. Chem.* **65**, 25–29 (1961).
- <sup>39</sup>M. M. Dubinin, "Microporous structures and adsorption properties of carbonaceous adsorbents," *Carbon* **21**, 359–366 (1983).
- <sup>40</sup>S. Yaghoubian, "Initiation of condensation of toluene and octane vapours on a Si surface," *RSC Adv.* **10**, 16291–16301 (2020).
- <sup>41</sup>X. Wei, C.-M. Wu, and Y.-R. Li, "Atomistic investigation on the kinetic behavior of vapour adsorption and cluster evolution using a statistical rate theory approach," *Phys. Chem. Chem. Phys.* **23**, 18058–18067 (2021).
- <sup>42</sup>X. Wei, C.-M. Wu, and Y.-R. Li, "Characterizing on the interfacial thermal transport through adsorption clusters and vibrational behaviors," *Int. J. Heat Mass Transfer* **183**, 122086 (2022).
- <sup>43</sup>X. Wei, C.-M. Wu, and Y.-R. Li, "Molecular insight into the formation of adsorption clusters based on the zeta isotherm," *Phys. Chem. Chem. Phys.* **22**, 10123–10131 (2020).
- <sup>44</sup>F. Duan, I. Thompson, and C. A. Ward, "Statistical rate theory determination of water properties below the triple point," *J. Phys. Chem. B* **112**, 8605–8613 (2008).
- <sup>45</sup>S. Saber, "The transition of adsorbed water vapour on silica to adsorbed water," Master's thesis, University of Toronto, 2018.
- <sup>46</sup>A. W. Fejes Clark, "The effect of adsorption on energy transport at a solid–vapour interface," Master's thesis, University of Toronto, 2014.
- <sup>47</sup>W. Wagner and A. Pruß, "The IAPWS formulation 1995 for the thermodynamic properties of ordinary water substance for general and scientific use," *J. Phys. Chem. Ref. Data* **31**, 387–535 (2002).
- <sup>48</sup>L. J. Schlangen, *Adsorption and Wetting: Experiments, Thermodynamics and Molecular Aspects* (Schlangen, 1995).
- <sup>49</sup>J. Taylor, *An Introduction to Error Analysis: The Study of Uncertainties in Physical Measurements*, ASMSU/Spartans.4.Spartans Textbook (University Science Books, 1997).
- <sup>50</sup>S. Brunauer, P. H. Emmett, and E. Teller, "Adsorption of gases in multimolecular layers," *J. Am. Chem. Soc.* **60**, 309–319 (1938).
- <sup>51</sup>V. P. Carey, *Liquid–Vapor Phase-Change Phenomena: An Introduction to the Thermophysics of Vaporization and Condensation Processes in Heat Transfer Equipment* (CRC Press, 2020).
- <sup>52</sup>H. B. Callen, *Thermodynamics and an Introduction to Thermostatistics*, 2nd ed. (John Wiley & Sons, Inc., 1985).
- <sup>53</sup>E. Chibowski, L. Holysz, G. A. M. Kip, A. van Silfhout, and H. J. Busscher, "Surface free energy components of glass from ellipsometry and zeta potential measurements," *J. Colloid Interface Sci.* **132**, 54–61 (1989).
- <sup>54</sup>D. B. Asay and S. H. Kim, "Evolution of the adsorbed water layer structure on silicon oxide at room temperature," *J. Phys. Chem. B* **109**, 16760–16763 (2005).
- <sup>55</sup>J.-B. d'espinoise de la Caillerie, M. R. Aimeur, Y. E. Kortobi, and A. P. Legrand, "Water adsorption on pyrogenic silica followed by <sup>1</sup>H MAS NMR," *J. Colloid Interface Sci.* **194**, 434–439 (1997).
- <sup>56</sup>L. T. Zhuravlev and A. V. Kiselev, "Surface concentration of hydroxyl groups on amorphous silicas having different specific surface areas," in *Surface Area Determination*, edited by D. Everett and R. Ottewill (Butterworth-Heinemann, 1970), pp. 155–160.
- <sup>57</sup>L. T. Zhuravlev, "Concentration of hydroxyl groups on the surface of amorphous silicas," *Langmuir* **3**, 316–318 (1987).
- <sup>58</sup>R. M. Pashley and J. A. Kitchener, "Surface forces in adsorbed multilayers of water on quartz," *J. Colloid Interface Sci.* **71**, 491–500 (1979).
- <sup>59</sup>B. V. Derjaguin and Z. M. Zorin, "Optical study of the adsorption and surface condensation of vapours in the vicinity of saturation on a smooth surface," *Prog. Surf. Sci.* **40**, 83–117 (1992).
- <sup>60</sup>A. L. Sumner, E. J. Menke, Y. Dubowski, J. T. Newberg, R. M. Penner, J. C. Hemminger, L. M. Wingen, T. Brauers, and B. J. Finlayson-Pitts, "The nature of water on surfaces of laboratory systems and implications for heterogeneous chemistry in the troposphere," *Phys. Chem. Chem. Phys.* **6**, 604–613 (2004).
- <sup>61</sup>M. L. Gee, T. W. Healy, and L. R. White, "Hydrophobicity effects in the condensation of water films on quartz," *J. Colloid Interface Sci.* **140**, 450–465 (1990).
- <sup>62</sup>W. R. Birch, M. A. Knewton, S. Garoff, R. M. Suter, and S. Satija, "Structure of precurving thin films of an anionic surfactant on a silicon oxide/silicon surface," *Langmuir* **11**, 48–56 (1995).
- <sup>63</sup>R. R. Mazzocco and P. C. Wayner, "Aqueous wetting films on fused quartz," *J. Colloid Interface Sci.* **214**, 156–169 (1999).

- <sup>64</sup>D. Grant and E. C. Salthouse, "The surface resistance of glass during the initial stages of dew formation on a cooled surface," *J. Phys. D: Appl. Phys.* **10**, 201 (1977).
- <sup>65</sup>M. Jakob, "Heat transfer in evaporation and condensation II," *Mech. Eng.* **58**, 729–740 (1936).
- <sup>66</sup>A. Majumdar and I. Mezic, "Instability of ultra-thin water films and the mechanism of droplet formation on hydrophilic surfaces," *J. Heat Transfer* **121**, 964–971 (1999).
- <sup>67</sup>H. M. Cassel, "Condensation and supersaturation of adsorbed phases," *J. Chem. Phys.* **12**, 115–116 (1944).
- <sup>68</sup>H. M. Cassel, "Cluster formation and phase transitions in the adsorbed state," *J. Phys. Chem.* **48**, 195–202 (1944).
- <sup>69</sup>T. L. Hill, *Theory of Physical Adsorption* (Academic Press, 1952), pp. 211–258.
- <sup>70</sup>N. Narayanaswamy, "Zeta adsorption isotherm: Surface area determination and kinetics of vapour adsorption," Ph.D. thesis, University of Toronto, 2022.